J. Fluid Mech. (2011), *vol.* 667, *pp.* 369–402.
doi:10.1017/S0022112010004489

Gravity-induced collisions of spherical drops covered with compressible surfactant

ALEXANDER Z. ZINCHENKO[1]†, MICHAEL A. ROTHER[2] AND ROBERT H. DAVIS[1]

[1]Department of Chemical and Biological Engineering, University of Colorado, Boulder, CO 80309-0424, USA

[2]Department of Chemical Engineering, University of Minnesota Duluth, Duluth, MN 55812-3025, USA

(Received 29 December 2009; revised 19 August 2010; accepted 20 August 2010)

Gravity-induced collisions of two spherical drops covered with an insoluble surfactant at low Reynolds numbers are considered. Unlike in previous collision studies, the present work accounts for nonlinear coupling between the surfactant distribution and drop hydrodynamics by solving the full unsteady convective–diffusion equation for the surfactant transport. Our method includes high-order three-dimensional multipole expansions for hydrodynamics and a Galerkin-type approach for the surfactant transport with implicit marching. The efficiency of the algorithm allows for calculating thousands of trajectories to very close contact and determining the collision efficiency (related to the critical initial horizontal offset) by trial and error. The solution is valid for arbitrary surface Péclet (Pe_s) and Marangoni (Ma) numbers and sets limitations on approximations used in prior work for collision-efficiency calculations. Two limiting cases are observed: at small Pe_s or large Ma, the variation in surfactant coverage is small, and the results for the incompressible surfactant model are recovered, while for large Pe_s and small Ma, the collision efficiency approaches the clean-interface value. For moderate drop-size ratios (radius ratio $k \leqslant 0.5$), the results generally fall between these limits. At larger size ratios, however, the collision efficiency may even exceed the geometrical Smoluchowski limit for both drops and bubbles. Moreover, with even moderate redistribution of the surfactant, equal-sized drops can move relative to one another and collide. These novel effects do not exist for clean drops or drops covered with an incompressible surfactant, and they are due to the nonlinear coupling between surfactant dynamics and flow. This surfactant-enhanced coalescence takes place, for example, in a physical system of air bubbles in water if the surfactant surface concentration is dilute ($\Gamma \approx 1 \times 10^{-9}$ mol m^{-2}, much smaller than the typical maximum-packing value of 10^{-5}–10^{-6} mol m^{-2}).

Key words: breakup/coalescence, drops and bubbles, emulsions

1. Introduction

Surfactants continue to be employed in newer and more sophisticated capacities, and their use can only be expected to increase in the upcoming decades (Porter 1990; Karsa 2000). More recent applications include microfluidics (Nguyen & Werely 2002;

† Email addresses for correspondence: alexander.zinchenko@colorado.edu, mrother@d.umn.edu, robert.davis@colorado.edu

Stone, Stroock & Ajdari 2004), where a drop can serve as a mixing or metering device (Cristini & Tan 2004) through coalescence and breakup. On a larger scale, the proper understanding of the effect of surfactants on the behaviour of emulsions, a problem of enormous everyday significance, requires fundamental investigation into their role in droplet interactions. In this work, we consider the gravitational motion of two spherical drops with negligible inertia in the presence of a bulk-insoluble, non-ionic surfactant. The goal of the analysis is to determine collision efficiencies under conditions when significant redistribution of the surfactant on the drop interfaces may occur.

We employ a linear relationship ('ideal gas') between interfacial tension and surfactant concentration. Nonlinear models (Chen & Stebe 1996) are most appropriate for high surfactant concentrations, but they would increase the number of parameters and are not considered herein. The ideal-gas equation of state is valid at low surfactant surface concentrations, but this regime is important because even small amounts of surfactant are sufficient to immobilize the drop interfaces (Chesters & Bazhlekov 2000). Moreover, with small amounts of adsorbed surfactant, it is possible to avoid the complications of surface viscosity (Pozrikidis 1994; Li 1996; Valkovska, Danov & Ivanov 1999, 2000). The linear model may also hold for non-dilute systems with small variations in the surfactant concentration (Bławzdziewicz, Wajnryb & Loewenberg 1999*b*). The case of bulk-insoluble non-ionic surfactants obeying the linear law has practical relevance for modelling the behaviour of compatibilizers and of soluble surfactants, when the diffusive exchange between bulk and interface is slow (Chesters & Bazhlekov 2000).

For a single spherical drop or bubble in the presence of surfactants, early theoretical work was done primarily for buoyancy-driven motion (Frumkin & Levich 1947; Levich 1962). These and subsequent studies have revealed several limiting cases: a non-retarded fluid velocity profile (Wasserman & Slattery 1969; Saville 1973; Agrawal & Wasan 1979; Harper 1988, 2007), a uniformly retarded fluid velocity profile (Levich 1962; Holbrook & LeVan 1983*a*,*b*), a stagnant cap (Griffith 1962; Sadhal & Johnson 1983; Cuenot, Magnaudet & Spennato 1997; Li & Mao 2001; Alves, Orvalho & Vasconcelos 2005) and a completely stagnant interface (Griffith 1962; Takemura 2005). Considerable attention has been given to experiments on a single drop or bubble in buoyancy to determine the effect of surfactants on the settling velocity or mass-transfer rate (Garner & Skelland 1955; Elzinga & Banchero 1961; Griffith 1962; Horton, Fritsch & Kintner 1965; Beitel & Heidegger 1971; Edge & Grant 1972; Yamaota & Ishii 1987; He, Maldarelli & Dagan 1991; Fdhila & Duineveld 1996; Zhang & Finch 2001).

In the limit of an incompressible surfactant film (Frumkin & Levich 1947; Levich 1962), two surfactant-covered drops interacting in a variety of flows have also been studied. Surfactant coverage is called 'incompressible' based on analogy with incompressible flow, where an infinitesimal change in density corresponds to a large pressure variation. In this case, finite differences in interfacial tension occur as a result of very small changes in surfactant concentration. Thus, the limit of incompressible surfactant is the same as the limit of nearly uniform surfactant surface coverage. As shown by the scaling arguments of Bławzdziewicz *et al.* (1999*b*), incompressible surfactants have physical importance, especially for small drops. The advantages of studying nearly uniform surfactant coverage include reduction of the parameter space by one, since the Marangoni and the surface Péclet numbers are combined into a single retardation parameter, and a relative ease of analysis, since the problem remains linear.

Zinchenko (1983) calculated the collision efficiency for two clean spherical drops with arbitrary drop-to-medium viscosity ratio in gravity-induced motion. Bispherical

coordinates and twin multipole expansions were employed for calculating drop mobilities along and normal to the line of centres, respectively. Bławzdziewicz *et al.* (1999*b*) considered collisions of two contaminated bubbles with incompressible surfactant in Brownian motion and linear flows. Rother & Davis (2004) studied gravitational interactions and collisions of two drops with incompressible surfactant for arbitrary viscosity ratio. Rother (2009) performed a similar analysis for spherical drops undergoing thermocapillary motion in the presence of surfactant. The experimental work of Hudson, Jamieson & Burkhart (2003) on two contaminated drops in shear flow confirmed the usefulness of the theoretical results of Bławzdziewicz *et al.* (1999*b*), probed the limits of the incompressible model, and made modifications for the more general surfactant-coverage case.

Also, some research has been done concerning spherical drops with compressible surfactant. Bławzdziewicz, Vlahovska & Loewenberg (2000) considered a rheological response of a single drop in a dilute emulsion in linear flows when redistribution of surfactant was possible but surface diffusion was neglected, and Vlahovska, Bławzdziewicz & Loewenberg (2002) extended the analysis to time-dependent flows. Cristini, Bławzdziewicz & Loewenberg (1998) performed local lubrication analysis for near-contact motion of two spherical drops with non-diffusing surfactant. Two-time-scales behaviour for film thinning was predicted, depending on the parameters. It should also be noted that important work has been done on film drainage between two slightly deformable drops with surfactants (Chesters & Bazhlekov 2000; Yeo *et al.* 2001; Danov, Valkovska & Ivanov 1999). In general, such work is restricted to axisymmetric, near-contact motion.

Relevant experiments have been conducted on the surfactant-like effect of compatibilizer on two polymer drops in linear flow under conditions when the flow is Newtonian (Hu, Pine & Leal 2000; Park, Baldessari & Leal 2003; Hudson *et al.* 2003). In experiments on dilute emulsions in shear flow in the presence of surfactants (Mousa & van de Ven 1991; Nandi, Mehra & Khakhar 1999; Hudson *et al.* 2003), results for the drop-size distribution were used to determine the collision efficiency via population dynamics.

Herein, we study, for the first time, the collision efficiency of two spherical drops covered with *compressible* surfactant in three-dimensional gravitational motion. The main motivation was to identify parameter ranges, where the droplet behaviour can be effectively characterized by treating the interfaces as having small variations from uniform surfactant coverage, or as being free of surfactant altogether. Thus, the present solution, valid at arbitrary surface Péclet and Marangoni numbers, clarifies the range of validity of prior solutions (Zinchenko 1982; Rother & Davis 2004) based on clean-surface and incompressible-surfactant models, respectively. Even more important, nonlinear coupling between surfactant and hydrodynamics, due to surfactant compressibility, leads to a new qualitative effect of enhanced collisions (coalescence). A curious analogy with the phenomenon of deformation-enhanced coalescence (Manga & Stone 1993, 1995) is observed, although the two mechanisms are very different. The assumptions behind the model, problem formulation and method of solution are the subject of §§ 2 and 3, respectively. Results and discussion are found in § 4 and concluding remarks in § 5.

2. Formulation of the problem

Consider the gravity-induced motion of two drops in an immiscible and unbounded fluid at low Reynolds numbers. The drops have the same density ρ^{int}, viscosity μ^{int},

different radii a_1 and a_2 (with $a_1 < a_2$) and sediment in the matrix fluid of density ρ^e and viscosity μ^e. Without a loss of generality, $\rho^{int} > \rho^e$ is assumed, so the drops move downward, the larger drop settling faster. The surface tension, σ, is assumed to be large enough to neglect drop deformation. The fluids inside and outside the drops are Newtonian, so that quasi-steady Stokes equations apply

$$\mu\nabla^2\boldsymbol{u} = \nabla p, \quad \nabla\cdot\boldsymbol{u} = 0, \tag{2.1}$$

for the fluid velocity $\boldsymbol{u}$ and dynamic pressure p inside and outside the drops. The fluid is quiescent at infinity ($\boldsymbol{u} \to \boldsymbol{0}$). Usual boundary conditions are the velocity continuity and no-flux on the drop surfaces S_1 and S_2

$$\boldsymbol{u}^e = \boldsymbol{u}^{int}, \quad (\boldsymbol{u}^e - \boldsymbol{V}_\gamma)\cdot\boldsymbol{n} = 0, \quad \boldsymbol{x}\epsilon S_\gamma, \quad \gamma = 1, 2, \tag{2.2}$$

where $\boldsymbol{V}_\gamma$ is the velocity of the drop centre and $\boldsymbol{n}$ is the outward normal to S_γ; indices e and int mark the quantities related to the exterior and interior phases, respectively. The drops are covered with an insoluble surfactant with surface concentration, Γ, governed by the convective–diffusion equation

$$\frac{\partial\Gamma}{\partial t} + \nabla_S\cdot(\Gamma\boldsymbol{u}^* - D_s\nabla\Gamma) = 0. \tag{2.3}$$

Here, D_s is the surface diffusion coefficient (the same for both drops), $\partial\Gamma/\partial t$ is the Euler derivative in a reference frame moving with the drop centre $\boldsymbol{O}_\gamma$, $\boldsymbol{u}^*$ is the fluid velocity relative to this frame ($\boldsymbol{u}^* \neq \boldsymbol{u} - \boldsymbol{V}_\gamma$, see § 3) and ∇_S is the surface nabla operator. The hydrodynamical and surfactant problems are coupled through the transport equation (2.3) and the interfacial stress balance

$$\boldsymbol{\Pi}_\tau^e - \boldsymbol{\Pi}_\tau^{int} = -\nabla_S\sigma, \quad \boldsymbol{x}\epsilon S_\gamma, \tag{2.4}$$

where $\boldsymbol{\Pi}_\tau$ is the tangential stress. The surface viscosity is neglected. Among possible relations $\sigma(\Gamma)$ between the surface tension, σ, and surfactant concentration, we choose the simplest linear law $\sigma = \sigma_o - RT\Gamma$, where σ_o is the clean-surface value, R is the universal gas constant and T is the absolute temperature (assumed constant). This form of $\sigma(\Gamma)$ is appropriate for non-ionic surfactants at low surface coverage in the absence of long-range interactions (Levich 1962). Colloidal interactions between the drops are neglected, and the hydrodynamical forces $\boldsymbol{F}_1$, $\boldsymbol{F}_2$ acting on the drops are constrained by the force balances

$$\boldsymbol{F}_\gamma + \tfrac{4}{3}\pi a_\gamma^3\Delta\rho\boldsymbol{g} = 0, \quad \Delta\rho = \rho^{int} - \rho^e. \tag{2.5}$$

The average surfactant concentration for each drop (preserved through the transport equation (2.3)) is Γ_{eq}. The drops are initially placed far away from each other, with the horizontal $d_\infty(\sim a_\gamma)$ and vertical $h_\infty(\gg a_\gamma)$ centre-to-centre offsets. To close the problem formulation, an initial condition for Γ at $t = 0$ is required, which we take in the simplest form $\Gamma = \Gamma_{eq}$; all results are found to be independent of h_∞, and alternative forms of the initial condition would not be advantageous.

The main quantity of interest from the solution is the critical offset d_∞^* demarcating relative trajectories leading to collision and separation; the related collision efficiency is defined as $E = [d_\infty^*/(a_1 + a_2)]^2$. Knowing E (and velocities of isolated drops) allows one to predict coalescence rates (assuming that each collision leads to coalescence) and the evolution of the drop-size distribution in dilute sedimenting emulsions. Unlike for solid spheres, the interfacial mobility of drop surfaces makes collisions possible even without singular attractive van der Waals forces, owing to weaker hydrodynamic

resistance to mutual approach (Zinchenko 1978, 1982; Davis, Schonberg & Rallison 1989).

In what follows, the problem and all the quantities are made non-dimensional by choosing a_2, $U = \Delta\rho g a_2^2/\mu^e$, a_2/U, $\mu^e U/a_2$ and Γ_{eq} as the scales for length, velocity, time, stress and surfactant concentration, respectively. In the non-dimensional form, the stress balance (2.4) takes the form $(\boldsymbol{\Pi}_\tau^e - \boldsymbol{\Pi}_\tau^{int}) = Ma\nabla_s\Gamma$, while the transport equation (2.3) acquires a factor of Pe_s^{-1} instead of D_s, where

$$Ma = \frac{RT\Gamma_{eq}}{\Delta\rho g a_2^2}, \quad Pe_s = \frac{\Delta\rho g a_2^3}{\mu^e D_s}, \tag{2.6}$$

are the Marangoni and the surface Péclet numbers, respectively. The non-dimensional critical offset, d_∞^*/a_2, found by trial and error, is a function of four non-dimensional parameters: Ma, Pe_s, size ratio $k = a_1/a_2$ and viscosity ratio $\widehat{\mu} = \mu^{int}/\mu^e$.

Two limiting cases have been studied in prior work. Zinchenko (1982) calculated the collision efficiency for clean drops as a function of k and $\widehat{\mu}$. In the other, more general limit of the so-called 'incompressible surfactant,' when $Ma \to \infty$, $Pe_s \to 0$ and $A = Ma\,Pe_s = O(1)$, deviations of the surfactant concentration from its average value Γ_{eq} are small, which allows one to replace (2.3) and (2.4) by

$$\nabla_S \cdot \left(\boldsymbol{\Pi}_\tau^e - \boldsymbol{\Pi}_\tau^{int} - A\boldsymbol{u}^*\right) = 0, \quad \nabla_S \times \left(\boldsymbol{\Pi}_\tau^e - \boldsymbol{\Pi}_\tau^{int}\right) = 0. \tag{2.7}$$

The clean-surface limit is recovered with $A = 0$. For the incompressible surfactant model, the collision efficiency of two drops in gravity-induced motion was calculated by Rother & Davis (2004); analogous collision efficiency calculations for bubble–bubble interactions in flow-induced motion (Bławzdziewicz *et al.* 1999*b*) were also based on the approximation (2.7). Note that, for the model (2.7), the solution of the transport equation (2.3) is bypassed, the whole problem is linear, instantaneous drop motion can be decomposed into translations along and normal to the line of centres, and the critical offset d_∞^* is found simply by integrating a combination of mobility functions for normal and transverse relative motion (Zinchenko 1982; Rother & Davis 2004) over all interparticle distances.

The incompressible surfactant approximation (2.7), though, is restrictive. In particular, it is clearly inadequate for low surfactant concentrations with $Ma \ll 1$ at large Pe_s. Since Marangoni and Péclet numbers can vary significantly, it would be of great theoretical and practical interest to determine instead the collision efficiencies from the solution of the full problem (2.1)–(2.5) at arbitrary Ma and Pe_s, with nonlinear coupling between surfactant and hydrodynamics through the transport equation (2.3). Such a solution, obtained for the first time in the present work, is far more complex than those in Zinchenko (1982) and Rother & Davis (2004). Namely, decomposition into normal and transverse motion can no longer be made in a practical fashion; determining critical offsets by trial and error and parametric analysis require thousands of trajectories to very close contact. A suitable algorithm is described in § 3.

3. Method of solution

Our method consists, at each time step, of (i) solving the hydrodynamical problem for two drops given the instantaneous surfactant distribution, (ii) updating the surfactant concentration through the transport equation and (iii) economical truncation of multipole expansions involved in (i) and (ii). These steps are detailed below.

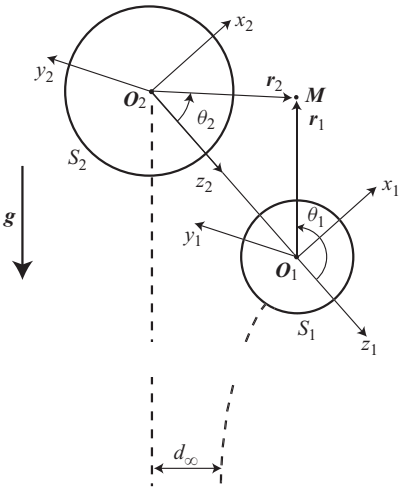

FIGURE 1. Schematic for two spherical drops settling under gravity (not to scale).

3.1. *Solution of the hydrodynamical problem*

It is convenient, and computationally most efficient, to work in two, moving and rotating coordinate systems (x_1, y_1, z_1), (x_2, y_2, z_2) centred at the drop centres $\boldsymbol{O}_1$, $\boldsymbol{O}_2$ and the z_1-, z_2-axes along the line of centres from sphere S_2 to S_1 (figure 1); these coordinate systems differ only by the translation. By definition, the x-axis lie in the plane span on the gravity vector and the line of centres. Along with $(x_\gamma, y_\gamma, z_\gamma)$, spherical coordinates $(r_\gamma, \theta_\gamma, \varphi_\gamma)$ (index γ labels drops 1 and 2, and related quantities) are used for an observation point M (figure 1)

$$x_\gamma = r_\gamma \sin\theta_\gamma \cos\varphi, \quad y_\gamma = r_\gamma \sin\theta_\gamma \sin\varphi, \quad z_\gamma = r_\gamma \cos\theta_\gamma, \tag{3.1}$$

where $\varphi = \varphi_1 = \varphi_2$ is the common angle of positive rotation about the z-axes.

The velocity field $\boldsymbol{u}^e$ outside the two spheres is sought as

$$\boldsymbol{u}^e = \boldsymbol{u}^1_- + \boldsymbol{u}^2_-, \tag{3.2}$$

where $\boldsymbol{u}^\gamma_-$ is a Stokes flow (to be found) regular everywhere outside the sphere with surface S_γ and represented by Lamb's (Happel & Brenner 1973) singular series:

$$\boldsymbol{u}^\gamma_- = \sum_{\nu=1}^{\infty} \left[\nabla \times \left(\boldsymbol{r}_\gamma \chi^\gamma_{-(\nu+1)} \right) + \nabla \Phi^\gamma_{-(\nu+1)} - \frac{(\nu-2) r_\gamma^2 \nabla p^\gamma_{-(\nu+1)}}{2\nu(2\nu-1)} + \frac{(\nu+1) p_{-(\nu+1)} \boldsymbol{r}_\gamma}{\nu(2\nu-1)} \right]. \tag{3.3}$$

The differential operations in (3.3) are with respect to $\boldsymbol{r}_\gamma = \boldsymbol{M} - \boldsymbol{O}_\gamma$, the negative-order solid harmonics are

$$\left.\begin{aligned} p^\gamma_{-(\nu+1)}(\boldsymbol{r}_\gamma) &= \sum_{m=-\nu}^{\nu} A^\gamma_{-(\nu+1),m} \left(\frac{a_\gamma}{r_\gamma} \right)^{\nu+1} Y_{\nu,m}(\boldsymbol{r}_\gamma), \\ \Phi^\gamma_{-(\nu+1)}(\boldsymbol{r}_\gamma) &= \sum_{m=-\nu}^{\nu} B^\gamma_{-(\nu+1),m} \left(\frac{a_\gamma}{r_\gamma} \right)^{\nu+1} Y_{\nu,m}(\boldsymbol{r}_\gamma), \\ \chi^\gamma_{-(\nu+1)}(\boldsymbol{r}_\gamma) &= \sum_{m=-\nu}^{\gamma} C^\gamma_{-(\nu+1),m} \left(\frac{a_\gamma}{r_\gamma} \right)^{\nu+1} Y_{\nu,m}(\boldsymbol{r}_\gamma), \end{aligned}\right\} \tag{3.4}$$

where $Y_{\nu,m}(\boldsymbol{r})$ is the standard normalized spherical harmonic

$$\left.\begin{aligned} Y_{\nu,m}(\boldsymbol{r}) &= \left[\frac{(2\nu+1)(\nu-m)!}{4\pi(\nu+m)!}\right]^{1/2} P_\nu^m(\cos\theta)\mathrm{e}^{\mathrm{i}m\varphi}, \quad (m \geqslant 0) \\ Y_{\nu,m}(\boldsymbol{r}) &= (-1)^m \overline{\boldsymbol{Y}}_{\nu,-m}(\boldsymbol{r}), \end{aligned}\right\} \tag{3.5}$$

$P_\nu^m(x) = (1-x^2)^{m/2} d^m P_\nu(x)/\mathrm{d}x^m$ is the associated Legendre function (in the definition of Korn & Korn 1968) and the overbar stands for complex conjugation; $a_1 = k$ and $a_2 = 1$ are the non-dimensional drop radii here and in the rest of the paper (unless otherwise stated). Complex coefficients in (3.4) obey

$$A^\gamma_{-(\nu+1),m} = (-1)^m \overline{A}^\gamma_{-(\nu+1),-m}, \quad \text{etc.} \tag{3.6}$$

to make (3.4) real valued. For the gravity-induced motion shown in figure 1, there is obvious symmetry of the solution about the $y = 0$ plane (with constraints on the coefficients in (3.4)), which is not assumed, though, in the method description below to make it general and suitable for other problems (e.g. flow-induced motion, without such symmetry).

The surface tension, σ, on the drop surfaces is assumed given by its expansions in spherical harmonics, equivalent to

$$Ma\,\Gamma\Big|_{S_\gamma} = \sum_{n=0}^{\infty} \sigma_n^\gamma, \quad \sigma_n^\gamma = \sum_{m=-n}^{n} \sigma_{n,m}^\gamma Y_{n,m}(\boldsymbol{r}_\gamma), \tag{3.7}$$

with complex coefficients satisfying (3.6) for $\sigma_{n,m}^\gamma$; the $n = 0$ term is insignificant here.

To proceed with applying the boundary conditions, the velocity field $\boldsymbol{u}_-^\gamma$ outside sphere S_γ is first expanded in the vicinity of the other sphere $S_{\gamma+1}$ (here and henceforth the index $\gamma+1$ is reduced by module 2, when $\gamma = 2$) as Lamb's regular series

$$\boldsymbol{u}_+^{\gamma+1} = \sum_{n=1}^{\infty} \left[\nabla \times \left(\boldsymbol{r}_{\gamma+1}\chi_n^{\gamma+1}\right) + \nabla\Phi_n^{\gamma+1} + \frac{(n+3)r_{\gamma+1}^2 \nabla p_n^{\gamma+1}}{2(n+1)(2n+3)} - \frac{n p_n^{\gamma+1}\boldsymbol{r}_{\gamma+1}}{(n+1)(2n+3)}\right], \tag{3.8}$$

with positive-order solid harmonics

$$\left.\begin{aligned} p_n^{\gamma+1} &= \sum_{m=-n}^{n} A_{n,m}^{\gamma+1} \left(\frac{r_{\gamma+1}}{a_{\gamma+1}}\right)^n Y_{n,m}(\boldsymbol{r}_{\gamma+1}), \\ \Phi_n^{\gamma+1} &= \sum_{m=-n}^{n} B_{n,m}^{\gamma+1} \left(\frac{r_{\gamma+1}}{a_{\gamma+1}}\right)^n Y_{n,m}(\boldsymbol{r}_{\gamma+1}), \\ \chi_n^{\gamma+1} &= \sum_{m=-n}^{n} C_{n,m}^{\gamma+1} \left(\frac{r_{\gamma+1}}{a_{\gamma+1}}\right)^n Y_{n,m}(\boldsymbol{r}_{\gamma+1}), \end{aligned}\right\} \tag{3.9}$$

again with $A_{n,-m}^{\gamma+1} = (-1)^m \bar{A}_{n,m}^{\gamma+1}$, etc. The general re-expansion formulae from $A_{-(\nu+1),m}^\gamma$, etc to $A_{n,m}^{\gamma+1}$, etc exist (Mo & Sangani 1994), but they are very cumbersome and, when used in an arbitrary coordinate system, would have the $O(N^4)$ cost of operations (assuming a truncation bound $N = \max(\nu, n)$ and all azimuthal numbers m used). A crucial advantage of the 'axial coordinates' (with the polar z-axis along the re-expansion vector $\boldsymbol{O}_2\boldsymbol{O}_1$) is that the re-expansion relations greatly simplify, with splitting in the azimuthal number m, and the cost of this operation reducing to $O(N^3)$. The corresponding formulae in the axial coordinates for $m = 0$ may be taken from

Happel & Brenner (1973), while for $m=1$ and 2, they were derived by Zinchenko (1982). General relations for arbitrary m used herein follow from (3.61), (3.64) and (3.66) of Zinchenko & Davis (2000)

$$\left.\begin{aligned}
A^{\gamma+1}_{n,m} &= \sum_{\nu=|m|}^{\infty} J^{m,\gamma}_{\nu,n} A^{\gamma}_{-(\nu+1),m},\\
B^{\gamma+1}_{n,m} &= (-1)^{\gamma}\frac{\mathrm{i}m}{n} R_{12} \sum_{\nu=|m|}^{\infty} J^{m,\gamma}_{\nu,n} C^{\gamma}_{-(\nu+1),m} + \sum_{\nu=|m|}^{\infty} J^{m,\gamma}_{\nu,n} B^{\gamma}_{-(\nu+1),m}\\
&\quad - R_{12}^2 \sum_{\nu=|m|}^{\infty} \frac{(\nu-2)}{2\nu(2\nu-1)} J^{m,\gamma}_{\nu,n} A^{\gamma}_{-(\nu+1),m} + \frac{(-1)^{\gamma-1} R_{12} a_{\gamma+1}}{n}\left[\frac{(n-m)(n+m)}{(2n-1)(2n+1)}\right]^{1/2}\\
&\quad \times \sum_{\nu=|m|}^{\infty} \frac{\left[(n-1)(\nu-2)-(\nu+1)\right]}{\nu(2\nu-1)} J^{m,\gamma}_{\nu,n-1} A^{\gamma}_{-(\nu+1),m},\\
C^{\gamma+1}_{n,m} &= (-1)^{\gamma}\frac{\mathrm{i}m R_{12}}{n(n+1)} \sum_{\nu=|m|}^{\infty} \frac{1}{\nu} J^{m,\gamma}_{\nu,n} A^{\gamma}_{-(\nu+1),m} - \frac{1}{(n+1)} \sum_{\nu=|m|}^{\infty} \nu J^{m,\gamma}_{\nu,n} C^{\gamma}_{-(\nu+1),m},
\end{aligned}\right\} \tag{3.10}$$

(omitting terms with $1/\nu$ for $\nu=0$). Here, R_{12} is the centre-to-centre distance, and

$$J^{m,\nu}_{\nu,n} = (-1)^{n(\gamma-1)+\nu\gamma+m}\left[\frac{(2\nu+1)(n+\nu)!(n+\nu)!}{(2n+1)(\nu-m)!(\nu+m)!(n-m)!(n+m)!}\right]^{1/2}\left(\frac{a_{\gamma+1}}{R_{12}}\right)^{n}\left(\frac{a_{\gamma}}{R_{12}}\right)^{\nu+1}. \tag{3.11}$$

Somewhat obscurely, through recurrent relations for J-coefficients, only four independent sums over ν (instead of seven) need to be calculated for each n and m in (3.10) (cf. Zinchenko & Davis 2008 for regular-to-regular re-expansions).

The exterior field $\boldsymbol{u}^{\gamma}_{-}+\boldsymbol{u}^{\gamma}_{+}$, now represented as Lamb's general series near S_γ through (3.10), must match the interior field $\boldsymbol{u}^{int}$ inside S_γ via the boundary conditions, which gives, upon exclusion of $\boldsymbol{u}^{int}$, relations between the sets of harmonics ($p^{\gamma}_{-(\nu+1)}$, $\Phi^{\gamma}_{-(\nu+1)}$, $\chi^{\gamma}_{-(\nu+1)}$) and (p^{γ}_{ν}, Φ^{γ}_{ν}, χ^{γ}_{ν}) on the drop surface S_γ. Such relations have long been known for clean drops (Hetsroni & Haber 1978), including thermocapillary effects (Rother & Davis 1999) and for the limit of incompressible surfactant (Rother & Davis 2004); other authors (Cichocki, Felderhof & Schmitz 1988; Jones & Schmitz 1988; Bławzdziewicz *et al.* 1999*b*) preferred a different set of basis functions (other than Lamb's representation) to reach a similar goal of expressing $\boldsymbol{u}^{\gamma}_{-}$ via $\boldsymbol{u}^{\gamma}_{+}$. In a general case for surfactant considered herein, the surface-tension gradient generates simple additional terms (Rother & Davis 1999) to those in Hetsroni & Haber (1978), yielding

$$\left.\begin{aligned}
A^{\gamma}_{-(\nu+1),m} &= -\frac{\nu(2\nu-1)}{(\nu+1)(1+\widehat{\mu})}\left\{\frac{\widehat{\mu}}{2} A^{\gamma}_{\nu,m} + [2+\widehat{\mu}(2\nu+1)]\frac{\widetilde{B}^{\gamma}_{\nu,m}}{a_\gamma^2}\right\} - \frac{\nu(2\nu-1)}{(2\nu+1)(1+\widehat{\mu})}\frac{\sigma^{\gamma}_{\nu,m}}{a_\gamma},\\
B^{\gamma}_{-(\nu+1),m} &= \frac{\nu}{2(\nu+1)(1+\widehat{\mu})}\left\{\frac{[2-\widehat{\mu}(2\nu+1)]a_\gamma^2}{2(2\nu+3)} A^{\gamma}_{\nu,m} - \widehat{\mu}(2\nu-1)\widetilde{B}^{\gamma}_{\nu,m}\right\}\\
&\quad - \frac{\nu a_\gamma}{2(2\nu+1)}\frac{\sigma^{\gamma}_{\nu,m}}{(1+\widehat{\mu})},\\
C^{\gamma}_{-(\nu+1),m} &= -\frac{(\nu-1)(\widehat{\mu}-1)}{(\nu+2)+\widehat{\mu}(\nu-1)} C^{\gamma}_{\nu,m}.
\end{aligned}\right\} \tag{3.12}$$

The last of the equations (3.12) is unaffected by surfactant. These relations are conveniently derived in the reference frame moving with the centre of the drop S_γ (to take advantage of zero normal fluid velocity). Accordingly, $\widetilde{B}^\gamma_{\nu,m} = B^\gamma_{\nu,m}$ except for $\nu = 1$, when

$$\widetilde{B}^\gamma_{1,0} = B^\gamma_{1,0} - \left(\frac{4\pi}{3}\right)^{1/2} a_\gamma V^\gamma_3, \quad \widetilde{B}^\gamma_{1,1} = B^\gamma_{1,1} - \left(\frac{2\pi}{3}\right)^{1/2} a_\gamma \left(V^\gamma_1 - \mathrm{i}V^\gamma_2\right), \tag{3.13}$$

where $(V^\gamma_1,\ V^\gamma_2,\ V^\gamma_3)$ is a (yet unknown) drop velocity in coordinates $(x_\gamma,\ y_\gamma,\ z_\gamma)$. Coefficients $A^\gamma_{-2,m}$ are prescribed by the hydrodynamic forces acting on the drops (Happel & Brenner 1973): $\boldsymbol{F}_\gamma = -4\pi\nabla(r^3_\gamma p^\gamma_{-2})$.

Expansion of the solution in inverse powers of the centre-to-centre distance and computing a large number of coefficients has been a popular method for two-drop (Zinchenko 1982; Jones & Schmitz 1988; Bławzdziewicz *et al.* 1999*b*) and two-particle problems. The benefit of this approach is the analytical dependence of the mobility (resistance) functions on the surface separation, making subsequent trajectory analysis very efficient. In the present problem, though, such semi-algebraic techniques must be abandoned because of arbitrary surfactant distribution (3.7) and the need for calculating the fluid velocity $\boldsymbol{u}$ to use in the transport equation (2.3). Thus, the system (3.10), (3.12) should instead be solved numerically at each instantaneous configuration. Upon exclusion of $\widetilde{B}^\gamma_{1,m}$, successive substitutions into the right-hand side of (3.10) and (3.12) always provide convergent iterations for this mobility problem. This simple iterative scheme was found sufficient in the present calculations, with only a few iterations per time step even in near contact, since the solution at the preceding time step provides a good initial approximation.

In the present problem of gravity-induced collisions, the solution symmetry about the $y_\gamma = 0$ plane is additionally exploited to speed up simulations by avoiding complex arithmetics in the computations. Namely, the azimuthal expansions for p- and Φ-harmonics in (3.4), (3.9) are in $\cos m\varphi$, and for χ-harmonics in $\sin m\varphi$. Accordingly, C-coefficients are purely imaginary, while other coefficients are real. The force balances (2.5) take the form

$$A^\gamma_{-2,0} = 2\left(\frac{\pi}{27}\right)^{1/2} a_\gamma \cos\beta, \quad A^\gamma_{-2,1} = -\left(\frac{2\pi}{27}\right)^{1/2} a_\gamma \sin\beta, \tag{3.14}$$

where β is the angle between the centre-to-centre vector $\boldsymbol{O}_2\boldsymbol{O}_1$ and the gravity vector. Upon convergence of iterations, the drop velocities $\boldsymbol{V}^\gamma$ are found from (3.13).

3.2. *Solution of the surfactant transport equation*

It is most natural, and computationally convenient, to solve the surfactant transport equation (2.3) on each sphere S_γ in the reference frame coincident with the axial coordinate system $(x_\gamma,\ y_\gamma,\ z_\gamma)$ of figure 1. This reference frame translates with the drop centre velocity, $\boldsymbol{V}^\gamma$, and rotates with the angular velocity, $(V^1_1 - V^2_1)/R_{12}$, (about the y_γ-axis) both known from the solution of the hydrodynamical problem. The fluid velocity, $\boldsymbol{u}^*$, on S_γ relative to this frame is obtained from (3.2)–(3.4), (3.8)–(3.9) and the boundary conditions (3.12)

$$\left.\begin{aligned} \boldsymbol{u}^*(\boldsymbol{x}) &= a^2\nabla_S\Pi + a\nabla_S\Psi\times\boldsymbol{r}, \quad \Pi = \sum_{n=1}^{\infty}\sum_{m=0}^{n} b_{n,m}\mathscr{D}^m_n(\eta)\cos m\varphi, \\ \Psi &= \sum_{n=1}^{\infty}\sum_{m=1}^{n} c_{n,m}\mathscr{D}^m_n(\eta)\sin m\varphi, \end{aligned}\right\} \tag{3.15}$$

where the real coefficients are

$$\left.\begin{aligned} b_{n,m} &= \frac{(2-\delta_{m,0})}{(1+\widehat{\mu})}\left[\frac{(2n-1)}{(n+1)a^2}\,\widetilde{B}_{n,m}+\frac{1}{2(n+1)}\,A_{n,m}-\frac{\sigma_{n,m}}{(2n+1)a}\right], \\ c_{n,m} &= -\frac{2(2n+1)}{a[n+2+\widehat{\mu}(n-1)]}\,\mathrm{Im}(C_{n,m})-\left(\frac{8\pi}{3}\right)^{1/2}\frac{\left(V_1^1-V_1^2\right)}{R_{12}}\delta_{n,1}\delta_{m,1}, \end{aligned}\right\} \tag{3.16}$$

and δ (with indices) is the Kronecker delta. In (3.15) and (3.16) and the rest of this section, index γ labelling quantities related to drop S_γ ($\boldsymbol{r}^\gamma = \boldsymbol{x} - \boldsymbol{O}_\gamma$, drop radius a_γ, $\widetilde{B}^\gamma_{n,m}$, etc.) is omitted, for brevity; $\eta = \cos\theta$, and $\mathscr{D}^m_\nu(\eta)$ is the prefactor before $\exp(\mathrm{i}m\varphi)$ in (3.5).

An expansion for the surfactant concentration on S_γ is

$$\Gamma = \sum_{m=0}^{\infty}\Gamma_m(t,\eta)\cos m\varphi, \quad \Gamma_m = \sum_{n=m}^{\infty}\Gamma_{n,m}(t)\mathscr{D}^m_n(\eta), \tag{3.17}$$

with a simple relation $\sigma_{n,m} = Ma\,\Gamma_{n,m}/(2-\delta_{m,0})$ to the coefficients in (3.7). To advance $\Gamma_{n,m}$ from the convective–diffusion equation (2.3), the expansion

$$\nabla_S\cdot(\Gamma\boldsymbol{u}^*) = \sum_{n=0}^{\infty}\sum_{m=0}^{n} d_{n,m}\mathscr{D}^m_n(\eta)\cos m\varphi, \tag{3.18}$$

is also required. A similar nonlinear operation was encountered in the three-dimensional solution for a solitary surfactant-covered spherical drop in an unbounded linear flow (Bławzdziewicz *et al.* 2000; Vlahovska *et al.* 2002). The technique chosen therein was to substitute the expansions for Γ and $\boldsymbol{u}^*$ and then expand $\nabla_S\cdot(\Gamma\boldsymbol{u}^*)$ using 3-j symbols from quantum mechanics. This elegant semi-analytical approach is suitable and convenient for single-drop calculations, with the order n of harmonics not exceeding eight (Vlahovska *et al.* 2002). In the present problem, though, an alternative, substantially more economical method for computing $d_{n,m}$ is required to avoid prohibitive cost, since the necessary order n of harmonics may reach several hundred for drops in very close approach.

In addition to Γ_m, let

$$\left.\begin{aligned} b_m(\eta) &= \sum_{n=m}^{\infty} b_{n,m}\mathscr{D}^m_n(\eta), \quad c_m(\eta) = \sum_{n=m}^{\infty} c_{n,m}\mathscr{D}^m_n(\eta), \\ f_m(\eta) &= \sum_{n=m}^{\infty} n(n+1)b_{n,m}\mathscr{D}^m_n(\eta), \end{aligned}\right\} \tag{3.19}$$

(time dependence is assumed). Substituting (3.15) and (3.17) into (3.18), and performing differential operations in spherical coordinates, the convective term $\nabla_S\cdot(\Gamma\boldsymbol{u}^*)$ can be expressed as

$$\left\{\sum_j \Gamma_j'(\eta)\cos j\varphi\right\}\left\{\sum_k[(1-\eta^2)b_k'(\eta)-kc_k(\eta)]\cos k\varphi\right\}+\left\{\sum_j j\Gamma_j(\eta)\sin j\varphi\right\}$$
$$\times\left\{\sum_k\left[\frac{kb_k(\eta)}{1-\eta^2}-c_k'(\eta)\right]\sin k\varphi\right\}-\left\{\sum_j\Gamma_j(\eta)\cos j\varphi\right\}\left\{\sum_k f_k(\eta)\cos k\varphi\right\}, \tag{3.20}$$

and transformed to

$$\sum_m \Lambda_m(\eta)\cos m\varphi, \tag{3.21}$$

by straightforward series multiplication. Using orthogonality of spherical harmonics, the expansion coefficients $d_{n,m}$ take the form

$$d_{n,m} = 2\pi \int_{-1}^{1} \Lambda_m(\eta)\mathscr{D}_n^m(\eta)\mathrm{d}\eta, \tag{3.22}$$

and are evaluated by Gaussian quadrature, which requires the values of $\Gamma_j(\eta)$, $\Gamma_j'(\eta)$, $b_k(\eta)$, $b_k'(\eta)$, $c_k(\eta)$, $c_k'(\eta)$, $f_k(\eta)$ and $\mathscr{D}_n^m(\eta)$ at the zeros of a Legendre polynomial. If the order n of harmonics in (3.15)–(3.17), (3.22) is truncated by $n \leqslant N$, then the integrand in (3.22) may be shown to be a polynomial of degree $\leqslant 3N$, making the method exact with $3N$ quadrature points (in practice, half as many points sufficed). Coefficients $d_{n,m}$ are calculated at an $O(N^3)$ cost, which is reduced to $O(N^2M)$ if additional truncation $m \leqslant M \ll N$ (see §3.3) is made; for comparison, direct expansion (3.18) would be $O(N^5)$, and $O(N^3M^2)$ intensive, respectively. Our method for handling the nonlinear term $\nabla_S\cdot(\Gamma\boldsymbol{u}^*)$ is closer to solutions of full Navier–Stokes equations by Galerkin methods than to the approach of Vlahovska *et al.* (2002).

The surfactant concentration coefficients, $\Gamma_{n,m}$, are updated by a fully implicit scheme

$$\frac{\Gamma_{n,m}(t_{k+1}) - \Gamma_{n,m}(t_k)}{\Delta t} + d_{n,m} + \frac{n(n+1)}{Pe_s a^2}\,\Gamma_{n,m}(t_{k+1}) = 0, \tag{3.23}$$

with $\Gamma = \Gamma(t_{k+1})$ and $\boldsymbol{u}^* = \boldsymbol{u}^*(t_k)$ in the convective-term expansion (3.18). The initial condition is $\Gamma_{n,m} = (4\pi)^{1/2}\delta_{n,0}\delta_{m,0}$. Equation (3.23) is successfully solved for $\Gamma_{n,m}(t_{k+1})$ to very small surface separations ($\sim 10^{-4}a$) by simple iterations, with typically one to two iterations only per time step using $\Gamma_{n,m}(t_k)$ as an initial approximation. For comparison, a semi-implicit scheme, with $\Gamma = \Gamma(t_k)$ in (3.18), was observed to crash when the surface clearance reaches from one to a few per cent of the drop radii, which is not small enough for collision efficiency calculations.

The need for fully implicit solutions of the transport equation to improve stability is widely recognized in boundary-integral simulations for a single deformable surfactant-covered drop (e.g. Stone & Leal 1990; Li & Pozrikidis 1997; Eggleton, Tsai & Stebe 2001), although the methods used therein (tri-diagonal solvers for axisymmetric, and Zeidel iterations for three-dimensional problems discretized by surface meshing) do not apply to the present simulations. The non-dimensional time step Δt for (3.23) and for updating the drop positions (by a first-order Euler scheme) was chosen as

$$\Delta t = c_{\Delta t}\left(\frac{\delta}{2\delta + 1}\right)^{1/2}, \tag{3.24}$$

where $c_{\Delta t} =$ constant and δ (without indices) is the non-dimensional surface clearance. The form (3.24) dictates a nearly constant time step at large separations, with refinement in close contact. A value of $c_{\Delta t} = 0.04$ provided negligible time-integration error for all calculations.

3.3. *Economical truncation of the expansions*

Except for very large Péclet numbers with the stagnant-cap type of behaviour, the rates of convergence of the expansions for the fluid velocity and surfactant concentration are mostly affected by hydrodynamical interactions, and the necessary order n of harmonics increases without bound as the drops come to contact. For systematic

collision-efficiency analysis, when thousands of trajectories need to be calculated, it is essential to have automatic and (nearly) optimal truncation strategy at every mutual configuration S_1, S_2. Instead of $A^{\gamma}_{-(n+1),m}$,... etc., Euclidean norms are considered

$$A^{\gamma}_{-(n+1)} = \left[\sum_{m=-n}^{n} \left|A^{\gamma}_{-(n+1),m}\right|^2\right]^{1/2}, \quad \text{etc.} \tag{3.25}$$

Unlike $A^{\gamma}_{-(n+1),m}$, etc, the coefficients $A^{\gamma}_{-(n+1)}$, etc are rotationally invariant. Generalizing the analysis of Zinchenko (1994) for the present case of different radii a_1 and a_2, all the hydrodynamical coefficients in (3.4) and (3.9) can be shown to behave like

$$A^{\gamma}_{-(n+1)}, \quad A^{\gamma}_{n}, \text{ etc } \sim (q_\gamma)^n, \quad n \to \infty, \tag{3.26}$$

to within algebraic factors of $O(n^\alpha)$. Although the hydrodynamical problem is solved here by twin spherical expansions, the progression exponents q_γ are curiously related to the geometry of the bipolar (bispherical) coordinate system for S_1, S_2 (see Appendix) and have explicit expressions:

$$\left.\begin{aligned} q_1 &= \frac{R_{12}^2 + a_1^2 - a_2^2 - \left\{\left[R_{12}^2 - (a_1+a_2)^2\right]\left[R_{12}^2 - (a_1-a_2)^2\right]\right\}^{1/2}}{2R_{12}a_1}, \\ q_2 &= \frac{R_{12}^2 + a_2^2 - a_1^2 - \left\{\left[R_{12}^2 - (a_1+a_2)^2\right]\left[R_{12}^2 - (a_1-a_2)^2\right]\right\}^{1/2}}{2R_{12}a_2}. \end{aligned}\right\} \tag{3.27}$$

The result (3.27) is quite universal and describes the decay of multipole coefficients for any boundary-value problem in the two-sphere geometry, with Laplace or Stokes equations solved by twin spherical expansions. In contrast, the algebraic prefactors $O(n^\alpha)$ in (3.26) and related numerical coefficients are individual for each problem and difficult to derive. For simplicity, we accept the form (3.26) without prefactors, and the order of harmonics to retain on each drop S_γ is found as

$$n \leqslant N_\gamma, \quad N_\gamma \approx |\ln \varepsilon|/|\ln q_\gamma|, \tag{3.28}$$

where $\varepsilon \ll 1$ is a free parameter controlling the truncations (typically, $\varepsilon = 0.005$ in the present calculations). An additional limitation $n \geqslant n_{min}$ (with $n_{min} \sim 5$–10 for typical collision calculations at moderate Pe_s, but much larger, $n_{min} \sim 10^2$, in high-resolution examples of § 4 at very high Pe_s) is used to provide accuracy for well-separated drops. For drops of disparate radii, the bounds N_1 and N_2 are quite different; convergence is faster on the smaller drop. As the surface clearance δ tends to zero, the progression exponents behave like $q_\gamma = 1 - O(\delta^{1/2})$, so mutual approach to very small separations $\delta \sim 10^{-4}$ is handled with the order of multipoles reaching several hundred. For consistency, the order n of harmonics in the surfactant expansions (3.17) is truncated in the same way as for hydrodynamics (3.28). An alternative of using low-order surfactant expansions was found too crude in collision-efficiency calculations, nor does it expedite the overall numerical solution.

For clean drops (Zinchenko 1982) or drops with incompressible surfactant (Rother & Davis 2004) in gravity, instantaneous drop motion can be decomposed into translations along and normal to the line of centres, each problem requiring, respectively, $m = 0$ and $m = \pm 1$ only. In the present, more general case, due to nonlinear coupling between hydrodynamics and the surfactant transport through the convective term (3.18) and the three-dimensional character of the trajectories, one could expect all azimuthal numbers $|m| \leqslant n$ to be necessary. In contrast, and surprisingly, all our calculations in a wide range of parameters (§ 4) reveal that an

additional truncation $|m| \leqslant M$ with rather small M has a negligible effect on the trajectories and collision efficiency, even when the results differ considerably from the two limiting cases mentioned above. For large $Pe_s \sim 10^3$ and small Marangoni numbers, M up to 5 was necessary, while even $M = 3$ sufficed for moderate Pe_s. Accurate calculation of the surfactant distribution required larger values of M, but still not exceeding 7–9. In one example, with very high $Pe_s = 10^5$, values of $M \sim 20$ had to be used. This additional truncation $|m| \leqslant M$ (which obviously could not be made, had we chosen general coordinate systems with the z-axis not aligned with the line of centres) greatly expedites calculations. The success of the azimuthal truncation $|m| \leqslant M$ may be explained as follows. In principle, at any instantaneous configuration, the hydrodynamical problem can be decomposed into (i) interaction of two fixed drops under Marangoni stresses and (ii) motion of two clean drops with velocities $\boldsymbol{V}_1$ and $\boldsymbol{V}_2$. Presumably, problem (i) does not require very high-order multipoles, while problem (ii) requires $m = 0$ and $m = 1$ only. However, neither surfactant distribution in (i) nor drop velocities in (ii) is known *a priori*, and so we did not try to implement such a decomposition in the present algorithm.

3.4. *Performance of the algorithm*

Two examples with $Pe_s = 1000$, $Ma = 0.1$, $M = 5$, $c_{\Delta t} = 0.04$ and $\varepsilon = 0.005$ illustrate the performance of the code. The first case is for size ratio $k = 0.5$, viscosity ratio of $\widehat{\mu} = 2$, and initial non-dimensional horizontal $d_\infty = 0.35$ and vertical $h_\infty = 10$ centre-to-centre offsets. The near-critical relative trajectory reaches minimum surface separation of $\delta = 7.6 \times 10^{-4}$ before going back to infinity. The simulation took about 25 000 time steps (to the moment when δ is back at 3) and 6 min on a single processor of AMD PC with 2.8 GHz CPU. In the second example with $k = 0.9$, $\widehat{\mu} = 0.5$, $d_\infty = 2$ and $h_\infty = 10$, the drops collide. Simulation to separations $\delta = 3 \times 10^{-4}$ took about 20 000 time steps and 3.5 min of CPU time (only 12 s to reach $\delta = 0.01$). Solving the transport equation takes only 6 % of the overall cost, owing to the fast method for the convective term (3.18). The results with $M \leqslant 2$ are incorrect, even qualitatively, while $M = 5$ provides high accuracy. In the last example, the collision angle $\beta = 1.8305$ between the centreline and vertical is accurate to ~ 0.01 %. Simulations to such small separations $\delta \sim 10^{-4}$ are not redundant. For clean drops with $\widehat{\mu} = O(1)$, the resistance coefficient to mutual approach is known to behave like $\delta^{-1/2}$ (Zinchenko 1978, 1982; Davis *et al.* 1989), with $O(\delta^{1/2})$ contribution of separations smaller than δ to the collision efficiency. Van der Waals attractions, which can weaken the effect of the near-contact region for very small drops, are neglected in our analysis. Obviously, in the present formulation, it makes sense to perform simulations for only small and moderate viscosity ratios $\widehat{\mu}$, or else the near-contact contribution to the collision efficiency would be even larger.

4. Results

Several checks were performed on the present code. In figure 2, surfactant surface concentration profiles for bubbles ($\hat{\mu} = 0$) with centre-to-centre separations of $1000a_2$ are compared with results for isolated bubbles (Holbrook & LeVan 1983*b*). These authors investigated the limit of bulk-insoluble surfactant as part of a more general study on surfactant-induced retardation of the motion of a single drop. Their Eötvös number, *Eö*, and surface Péclet number, Pe_s^{HL}, are related to the corresponding

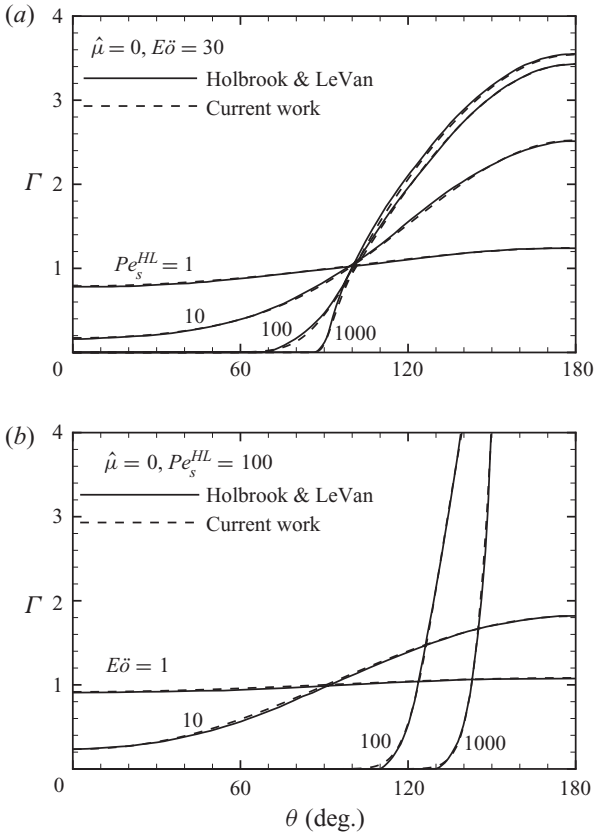

FIGURE 2. Comparison of the dimensionless surfactant profiles between the current work (dashed lines) and that of Holbrook & LeVan (1983*b*) (solid lines) for an isolated bubble in gravity. In (*a*) the surface Péclet number Pe_s^{HL}, as defined in Holbrook & LeVan (1983*b*), is varied between 1 and 1000 at a fixed Eötvös number of $E\ddot{o} = 30$, while in (*b*) curves are shown for $E\ddot{o}$ between 1 and 1000 with $Pe_s^{HL} = 100$.

parameters, Ma and Pe_s, of the current work by

$$Ma\,E\ddot{o} = 4, \qquad Pe_s = \frac{9}{4}\frac{(\widehat{\mu} + 2/3)}{(\widehat{\mu} + 1)} Pe_s^{HL}. \tag{4.1}$$

Excellent agreement in the dimensionless surfactant surface concentration, Γ, along the bubble surface is obtained over a wide range of surface Péclet (figure 2*a*) and Marangoni (figure 2*b*) numbers, where the angle θ is measured from the front stagnation point. In addition, our isolated bubble velocities (not shown) are nearly indistinguishable from those in Holbrook & LeVan 1983*b* over similar parameter ranges.

A second comparison was made for drop trajectories and surfactant profiles with our previous work (Rother *et al.* 2006) on surfactant effects on gravitational interactions of two deformable drops. The effect of deformation is shown in figure 3 in a series of images from relative trajectories at gravitational Bond numbers of $Bo = 0$, 1 and 2, from left to right, respectively, where

$$Bo = \frac{\Delta\rho g a_2^2}{\sigma_0}. \tag{4.2}$$

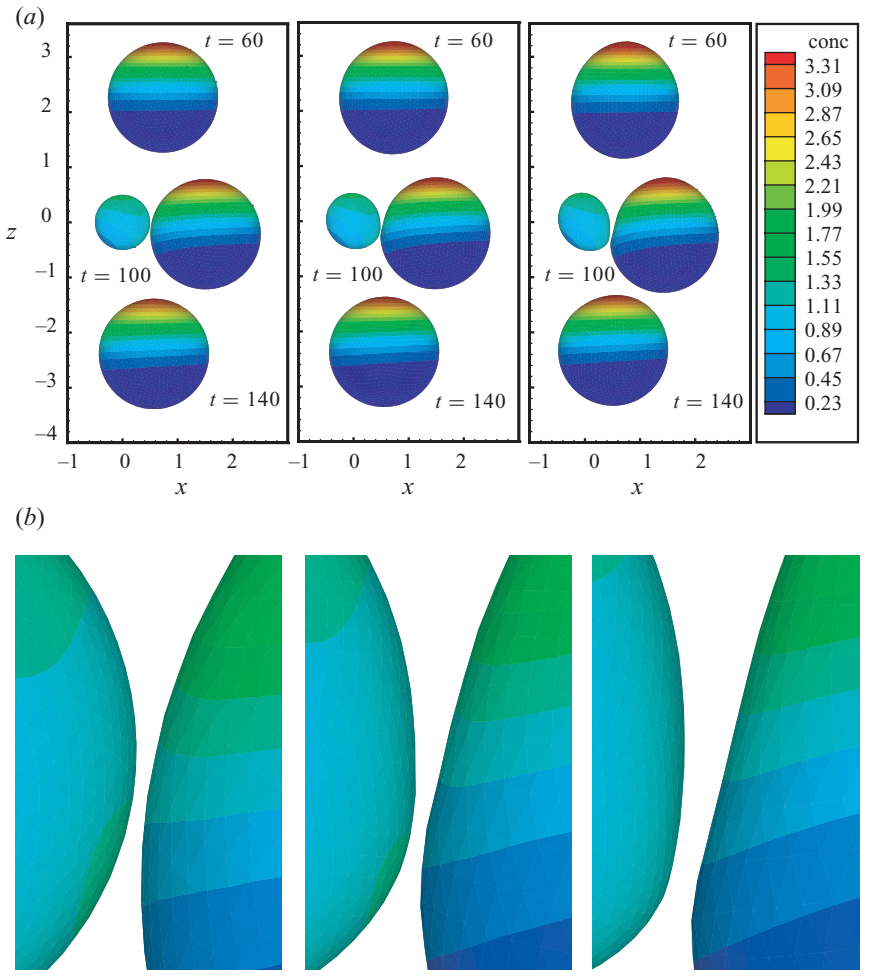

FIGURE 3. Images from relative trajectories of two surfactant-covered drops with $k = 0.5$, $\widehat{\mu} = 1$, $Pe_s = 100$, $Ma = 0.1$, and an initial separation of $d_\infty = 0.5$ and $h_\infty = 10$ at times of $t = 60$, 100 and 140, where the smaller drop is shown only at $t = 100$. From left to right, the Bond numbers are $Bo = 0$ (current work), 1, and 2, where the trajectories for deformable drops were determined from the algorithm of Rother, Zinchenko & Davis (2006). The images in the lower half of the figure are close-ups of the gap at $t = 100$. The colour contours indicate iso-concentration lines. The coordinates (x, z) (not to confuse with the intrinsic coordinates $(x^\gamma, y^\gamma, z^\gamma)$ of § 3) are centred at the smaller drop with the vertical z-axis.

The results for $Bo = 0$ were determined with the present code, while those for $Bo = 1$ and 2 were calculated using the boundary-integral algorithm from Rother *et al.* (2006). As the Bond number increases, the gap at $t = 100$ becomes larger, together with the amount of deformation, because of the greater resistance to film drainage. Moreover, the lubrication flow in the region of close approach becomes weaker. As a result, while there are patches of increased and decreased surfactant concentration on the smaller drop near the gap for $Bo = 0$ at $t = 100$ due to the interplay of the external and lubrication flows, these regions are smaller for $Bo = 1$ and have disappeared altogether at $Bo = 2$, at least to the sensitivity of the surfactant concentration contours shown.

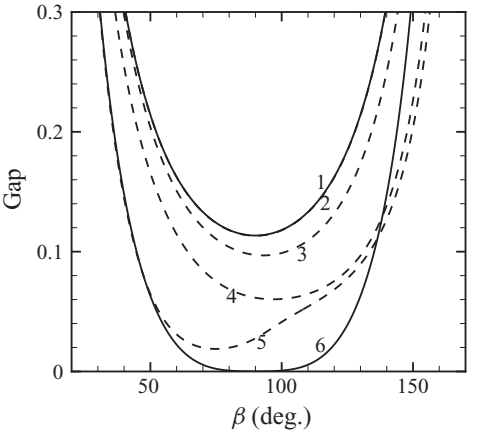

FIGURE 4. Relative trajectories with $k = 0.5$, $\widehat{\mu} = 1$ and initial separation of $d_\infty = 0.5$ and $h_\infty = 10$, shown as the gap versus the angle β between the drops' line of centres and vertical ($\beta \approx 0$ at the start). The upper solid curve (1) is for incompressible surfactant (Rother & Davis 2004) with retardation parameter $A = 10^4$, while the lower solid line (6) is a near-critical trajectory for clean drops (Zinchenko 1982) reaching separation $\delta = 1.1 \times 10^{-4}$. The four dashed lines are for compressible surfactant with 2: $Pe_s = Ma = 100$ (nearly coincident with curve 1); 3: $Pe_s = 10^4$, $Ma = 1$; 4: $Pe_s = 4 \times 10^4$, $Ma = 0.25$ and 5: $Pe_s = 10^5$, $Ma = 0.1$.

A final check on the present code is a comparison with the model for incompressible surfactant (Rother & Davis 2004). A surfactant film is incompressible in the limit of nearly uniform coverage. Scaling arguments (Bławzdziewicz *et al.* 1999*b*) show that there is small variation in surfactant surface coverage at small Pe_s or large Ma. In figure 4, relative trajectories are presented for values of the Marangoni and surface Péclet numbers, such that their product $A = Ma\,Pe_s = 10\,000$. The upper solid curve was determined from the incompressible surfactant model (Rother & Davis 2004), while the dashed curves mark trajectories from the present solution for compressible surfactant, where β is the angle between vertical and the drops' line of centres ($\beta \approx 0$ at the start). At $Pe_s = Ma = 100$, the trajectories for the two models coincide. Moreover, the images in figure 5(*a*) from the same interaction with $Pe_s = Ma = 100$ indicate that the coverage is indeed nearly uniform and that the Marangoni number is large enough for the surfactant film to be considered incompressible.

As the surface Péclet number increases and Marangoni number decreases, there is increasing divergence between the trajectories for the present solution and incompressible surfactant approximation in figure 4. The images from the interaction for $Pe_s = 4 \times 10^4$ and $Ma = 0.25$ in figure 5(*b*) show that there is significant variation in the surfactant concentration over the drop interfaces and that the incompressible model is no longer valid. For $Ma = 0.1$ and $Pe_s = 10^5$ (curve 5 of figure 4), the trajectory is even farther from the incompressible model limit and is practically coincident with that for clean drops until close approach. Even though the surfactant concentrations are highly non-uniform in this case, the Marangoni stresses are limited on most of the surfaces due to smallness of Ma. In near contact, though, details of surfactant distribution become important, and there is considerable deviation from the surfactant-free case, making the subsequent trajectory highly asymmetric about $\beta = 90°$. Additional calculations for $Ma = 0.1$ (not shown in figure 4) reveal that as Pe_s is reduced, the range of agreement with the clean-surface limit is extended to

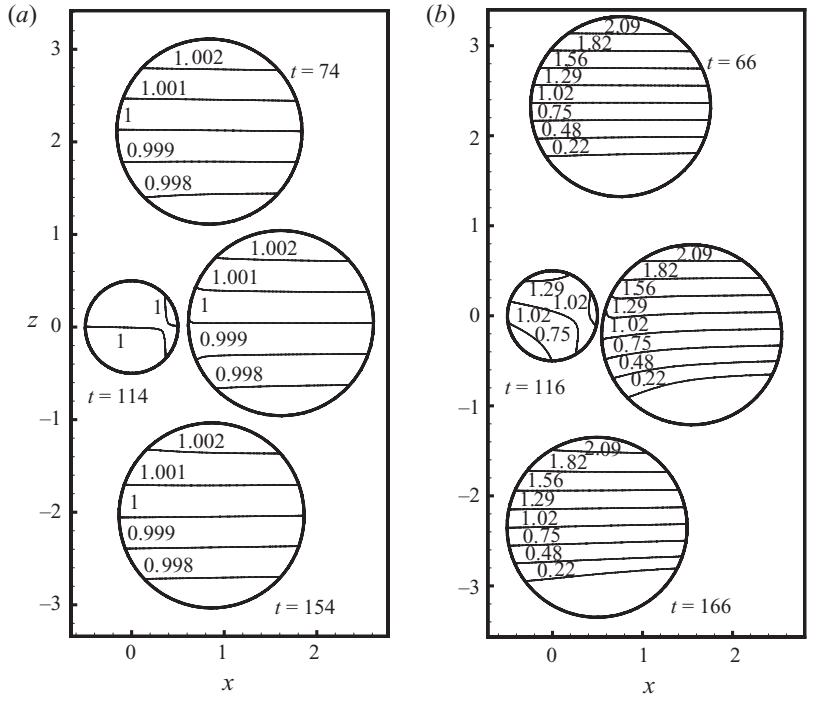

FIGURE 5. Images from relative trajectories of two surfactant-covered spherical drops with $k = 0.5$, $\widehat{\mu} = 1$, and an initial separation of $d_\infty = 0.5$ and $h_\infty = 10$ for (*a*) $Pe_s = Ma = 100$ at times of $t = 74$, 114 and 154 and (*b*) $Pe_s = 4 \times 10^4$ and $Ma = 0.25$ at $t = 66$, 116 and 166, where the smaller drop is shown only at the intermediate time. The contours indicate iso-concentration lines.

smaller gaps, and at $Pe_s \leqslant 0.1$ the whole curve $\delta(\beta)$ is practically indistinguishable from that for clean drops from figure 4.

As discussed later, for very high Péclet numbers $Pe_s \geqslant O(10^4)$ and $Ma \leqslant O(0.1)$, it is hard to resolve surfactant concentrations (and avoid non-physical, negative values of Γ) in areas almost depleted of surfactant. Global drop dynamics, however, is much less sensitive to these details, owing to the Galerkin type of the present algorithm. For the curve 5 of figure 4, with $Pe_s = 10^5$ and $Ma = 0.1$, refining truncation parameters (§ 3.3) $n_{min} = M = 20$, $\varepsilon = 0.005$ to $n_{min} = M = 70$, $\varepsilon = 0.001$ did not produce any detectable changes. However, $n_{min} = M = 10$ was unreliable (depending on ε) and $n_{min} = M = 5$ could never avoid divergence of iterations for the transport equation (2.3) in close approach. Due to these limitations and associated computational expenses, we could not focus on systematic three-dimensional collision-efficiency calculations (requiring many trials) at very high Pe_s. For $Pe_s = \infty$, our algorithm is not applicable (or, at least, would require a prohibitively large order of harmonics to work). A contemporary view (Eggleton, Pawar & Stebe 1999) is that the surface diffusion is typically very small and may be neglected, which is likely true for larger drops with finite deformations, but does not necessarily hold for small spherical drops considered herein, since the Péclet number (2.6) is proportional to the cube of the drop radius.

In figures 6–9, an investigation is made into the parameter space governing the dimensionless critical horizontal offset d_∞^* demarcating trajectories which lead to coalescence and separation of the drops. In all calculations, the initial vertical separation was $h_\infty = 1000$, and the drops were considered to have come into contact

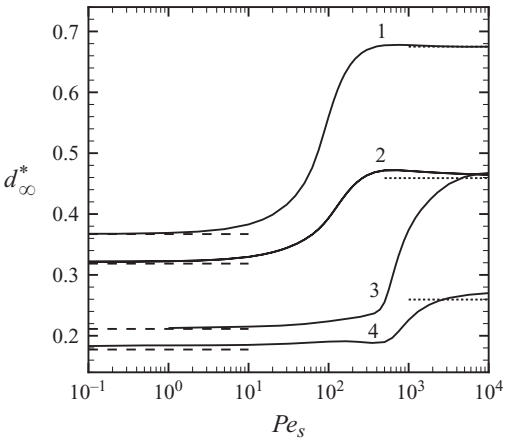

FIGURE 6. The critical horizontal offset from the present solution (solid lines) versus Péclet number at fixed values of $A = Pe_s Ma$; 1: $A = 10$, $\hat{\mu} = 0$; 2: $A = 10$, $\hat{\mu} = 1$; 3: $A = 100$, $\hat{\mu} = 1$; 4: $A = 100$, $\hat{\mu} = 5$. Size ratio $k = 0.5$. Short-dashed lines on the right are for clean drops (Zinchenko 1982) at viscosity ratios (top to bottom) $\hat{\mu} = 0$, 1 and 5. Long-dashed lines represent the limit of incompressible surfactant (from Rother & Davis 2004) with $Pe_s \to 0$, $Ma \to \infty$ at the same values of A and $\hat{\mu}$ as on the curves.

if the dimensionless gap δ reached 0.0001. We note that the collision efficiency, E_{12}, is related to the critical horizontal offset by

$$E_{12} = \left(\frac{d^*_\infty}{1+k} \right)^2. \tag{4.3}$$

In addition, in this study, coalescence is considered equivalent to collision.

Several approaches were taken to study surfactant effects on coalescence. In figure 6, the critical horizontal offset d^*_∞ from the present solution is shown as a function of the surface Péclet number, Pe_s, at fixed values of $A = Ma\,Pe_s$ (solid lines). For a moderate size ratio of $k = 0.5$, d^*_∞ varies between the result for incompressible surfactant (Rother & Davis 2004) at $Pe_s \to 0$, $M_a \to \infty$, and that for clean drops (Zinchenko 1982) at large Pe_s, where Ma is small and Marangoni stresses should disappear. Agreement with the two limiting cases is excellent for bubbles ($\widehat{\mu} = 0$) and good for drops with $\hat{\mu} = 1$. For a larger drop-to-medium viscosity ratio of $\hat{\mu} = 5$, some difference from the limiting cases is observed. This small discrepancy occurs because the collision criterion of $\delta = 0.0001$ in the present work is still too large to be accurate for drops with partially immobile interfaces at greater $\widehat{\mu}$ without van der Waals attractions. Note that the critical offset, and, hence, collision efficiency decrease with increasing $\hat{\mu}$ and that these collisions (to $\delta = 0$) will not occur for solid spheres ($\hat{\mu} \to \infty$) in the absence of van der Waals or other molecular attractions, due to the singular, non-integrable hydrodynamic resistance in this case.

In figures 7 and 8, the effect of the Marangoni number, surface Péclet number and size ratio on coalescence is considered, with the critical horizontal offset graphed versus the retardation parameter A. In figure 7, curves for compressible surfactant are shown at fixed values of Ma, while in figure 8 results at fixed Pe_s are presented. For a smaller size ratio of $k = 0.5$ and moderate viscosity ratio $\widehat{\mu} = 1$, curves with $Ma = 1$ (figure 7a) and $Pe_s = 1$ (figure 8a) almost coincide with those for nearly uniform coverage, and it is possible to define parameter ranges for which the incompressible-surfactant approximation is valid. From figure 7(a), the critical offset for $Ma = 0.01$

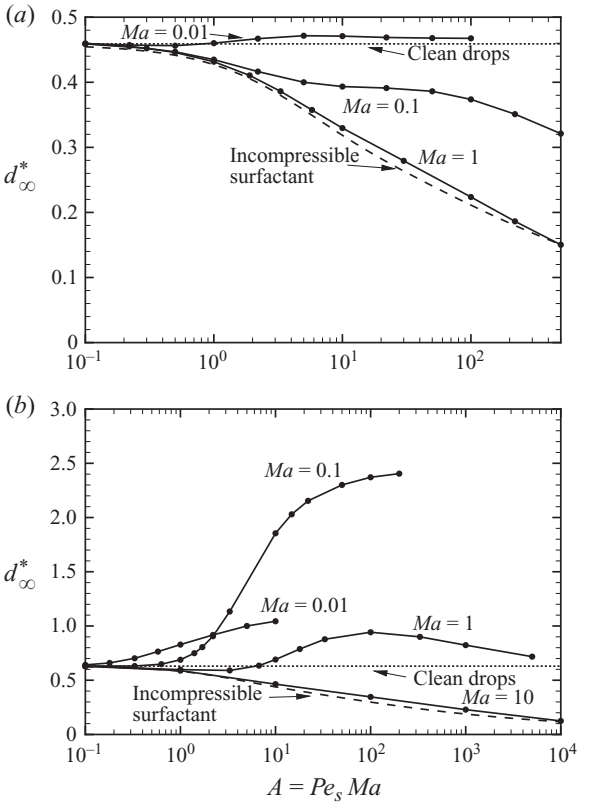

FIGURE 7. The critical horizontal offset versus the product $A = Pe_s Ma$ at $\widehat{\mu} = 1$ for size ratios (*a*) $k = 0.5$ and (*b*) $k = 0.9$. In both (*a*) and (*b*), the upper short-dashed horizontal line is for clean drops, while the lower long-dashed curve marks results for incompressible surfactant. Results for compressible surfactant from the present solution (solid lines) are shown at various values of the Marangoni number *Ma*.

matches that for clean drops, while from figure 8(*a*) the curves for $Pe_s = 100$ and 1000 begin to differ from that for clean drops at $Ma = O(0.01)$. Thus, some measure of applicability of the clean-drop approximation is also provided.

A maximum deviation between the two bounding limits occurs at $Ma = O(0.1)$. From figure 8(*a*) for $Pe_s = 100$ and 1000, d^*_∞ approaches the values for the incompressible surfactant model as $Ma \to 1$. The inset in figure 8(*a*) indicates that the present results for compressible surfactant actually dip below those for nearly uniform coverage before approaching them as $A \to 1000$. For the smallest Péclet number shown in figure 8, $Pe_s = 1$, incompressible surfactant is an excellent approximation in the whole range of Marangoni numbers.

The behaviour of drops at larger size ratios is much different than that observed for smaller k, as displayed in figures 7(*b*) and 8(*b*) for $k = 0.9$. The incompressible surfactant approximation is valid at $Ma = 10$ (figure 7*b*) and $Pe_s = 1$ (figure 8*b*). The results at $Ma \to 0$ still approach those for clean drops. However, even for $Ma = 0.01$ in figure 7(*b*), there is significant impact of surfactant compressibility on the critical offset. Most interestingly, as demonstrated in the curves for $Ma = 0.1$ (figure 7*b*) and $Pe_s = 100$ and 1000 (figure 8*b*), it is possible for the dimensionless critical offset to exceed the Smoluchowski limit of $d^*_\infty = 1 + k$ for straight trajectories. This

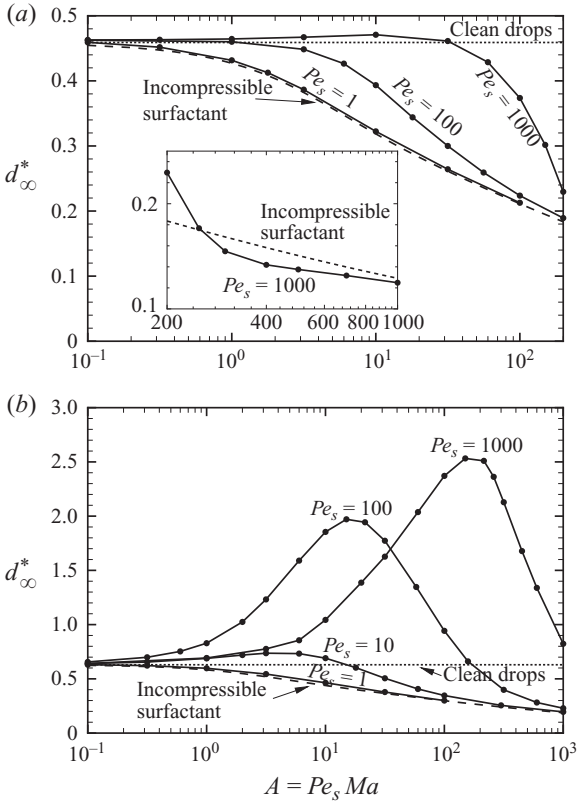

FIGURE 8. The critical horizontal offset versus the product $A = Pe_s Ma$ at $\widehat{\mu} = 1$ for size ratios (*a*) $k = 0.5$ and (*b*) $k = 0.9$. In both (*a*) and (*b*), the upper short-dashed horizontal line is for clean drops, while the lower long-dashed curve marks results for incompressible surfactant. Results for compressible surfactant (solid lines) are shown at various values of the surface Péclet number Pe_s. The inset in (*a*) is a continuation of the curve at $Pe_s = 1000$ in comparison with the incompressible surfactant model.

surfactant-enhanced coalescence observed at large size ratios is reminiscent of the deformation-induced coating and capture phenomena discovered by Manga & Stone (1993, 1995) for nearly equal-sized drops and studied later in detail by Zinchenko, Rother & Davis (1999). In the present problem, nonlinear coupling between surfactant and hydrodynamics, not captured by the incompressible surfactant model, is responsible for this behaviour.

One difference between the results for clean deformable drops at large Bond numbers and those for contaminated spherical drops is the effect of the viscosity ratio. Deformation-induced coating and capture are most prominent for bubbles. As the viscosity ratio increases, the effect of deformation on coalescence becomes weaker and is eventually masked by breakup and passthrough (Zinchenko *et al.* 1999; Kushner, Rother & Davis 2001) as $\widehat{\mu} \to O(1)$. However, for spherical drops in the presence of surfactant, results for the critical offset as a function of the size ratio are comparable for $\widehat{\mu} = 0$ and 1, as shown in figure 9. In fact, as $k \to 1$, d^*_∞ for drops ($\widehat{\mu} = 1$) becomes larger than that for bubbles ($\widehat{\mu} = 0$). For drops/bubbles with compressible surfactant at $Pe_s = 100$ and $Ma = 0.1$, the critical offset exceeds that for clean surfaces when $k > 0.7$ (figure 9) and appears to approach infinity as the size

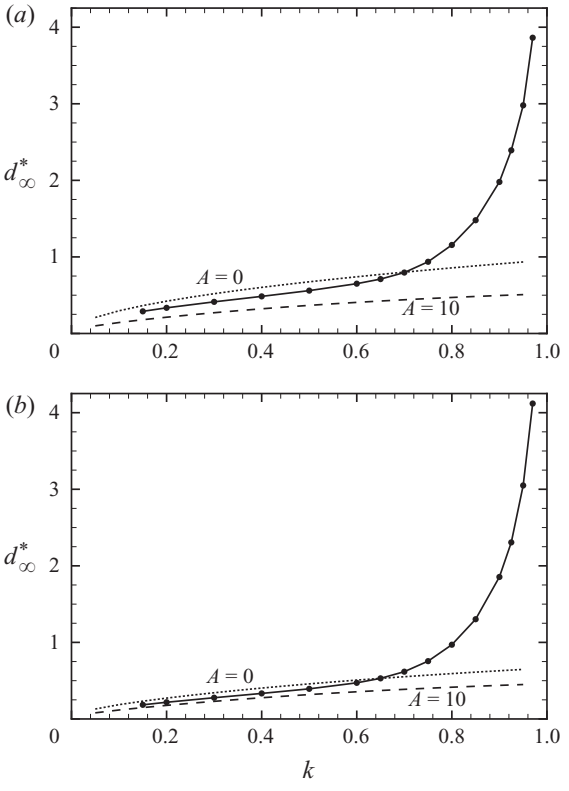

FIGURE 9. The critical horizontal offset versus the size ratio k at $Pe_s = 100$ and $Ma = 0.1$ for (a) bubbles ($\widehat{\mu} = 0$) and (b) drops ($\widehat{\mu} = 1$) with compressible surfactant (solid lines). In both (a) and (b), the upper short-dashed horizontal line is for clean drops ($A = 0$), while the lower long-dashed curve marks results for incompressible surfactant ($A = 10$).

ratio goes to unity. It should be noted, though, that two-drop mutual approach slows down as $k \to 1$, so in practice other weak mechanisms (e.g. collective interactions) may interfere with the collision process, unless the system is very dilute.

In figure 10, further study of surfactant-enhanced coalescence is made by considering the critical angle, β_{cr}, between vertical and the drops' line of centres at which the drops come into contact in the limiting trajectory (with $d_\infty = d^*_\infty$ far upstream). When the equations of motion remain linear, $\beta_{cr} = 90°$, as in the case of clean spherical drops or spherical drops covered with incompressible surfactant. However, for compressible surfactant, the problem is nonlinear, requiring solution of the full convective–diffusion equation, so the symmetry of non-colliding trajectories about $\beta = 90°$ is broken even in the absence of van der Waals forces, and significant deviation from $\beta_{cr} = 90°$ may occur. For drops ($\widehat{\mu} = 1$) at $Pe_s = 100$ and $Ma = 0.1$ in figure 10, the critical angle is slightly less than 90° for size ratios up to $k = 0.6$. When the drops are closer in size, the critical angle increases and reaches 180° at $k \to 1$. There are some minor errors in β_{cr}, especially as $k \to 1$, since this angle was found to be quite sensitive to the simulation parameters, and the tolerance in determining the critical horizontal offset was between 0.001 and 0.0001.

The phenomenon of enhanced coalescence is closely related to the behaviour of two equal-sized contaminated spherical drops in gravity. For clean surfaces or surfaces with incompressible surfactant, such a pair of drops would sediment as an aggregate

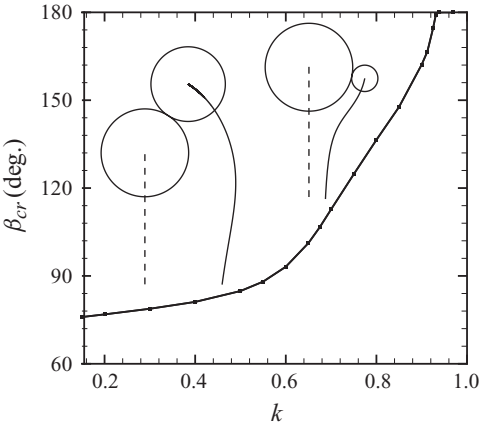

FIGURE 10. The critical angle, β_{cr}, demarcating trajectories which lead to separation and coalescence of the drops as a function of the size ratio k for $Pe_s = 100$, $Ma = 0.1$ and $\widehat{\mu} = 1$. The insets show two critical relative trajectories (with $\beta = \beta_{cr}$ at contact), for $k = 0.3$ (when $\beta_{cr} < 90°$) and $k = 0.85$ (with $\beta_{cr} > 90°$).

at constant interparticle distance without rotation, regardless of the initial separation. Without the incompressibility approximation, though, nonlinear coupling between the surfactant and hydrodynamics leads to a qualitatively different behaviour. In figure 11, motion of two equal drops is shown with the centreline (a) normal to and (b) along the gravity vector for $Ma = 0.1$ at different surface Péclet numbers; the inset in figure 11(a) indicates the surfactant concentration profiles in close approach for $Pe_s = 100$. As long as there is some variation in the surfactant concentration, the drops move towards one another and eventually collide, although for $Pe_s = 1$ the gap changes very slowly. For comparison, we note that in figure 11(b) two equal-sized drops with an initial gap of three drop radii reach a gap of 0.0001 at time $t \approx 1800$ for $Pe_s = 100$ and $Ma = 0.1$. However, if the size ratio is reduced to $k = 0.8$ for the same parameters and initial separation, the drops require only 90 dimensionless time units to reach the same final gap.

For the asymmetric motion from figure 11(a), a close-up (figure 12a) shows that the mutual approach does slow down, as the spheres come into contact, due to lubrication. The approach velocity $|\boldsymbol{V}_2 - \boldsymbol{V}_1|$ along the line of centres, though, displays an intriguing behaviour. In figure 12(b), $|\boldsymbol{V}_2 - \boldsymbol{V}_1|/\delta^{1/2}$ is shown versus gap δ for the near-contact stage. For clean drops under external forcing, this quantity would be $O(1)$ as $\delta \to 0$ (Zinchenko 1978, 1982; Davis *et al.* 1989). For contaminated drops from figure 11(a), $|\boldsymbol{V}_2 - \boldsymbol{V}_1|/\delta^{1/2}$ is almost constant in a wide range of small separations, but sharply increases as the spheres touch; $|\boldsymbol{V}_2 - \boldsymbol{V}_1|/\delta^{1/2} = O(1)$ at $\delta \to 0$ is still expected. A complex behaviour in figure 12(b) (with excellent numerical convergence and insensitive to initial conditions) indicates that the asymptotic analysis of 'surfactant-enhanced coalescence' must be difficult, requiring global solution.

Cristini *et al.* (1998) and Bławzdziewicz *et al.* (1999a) developed local near-contact lubrication analysis for two spherical drops with compressible non-diffusing surfactant pressed together by an external driving force. They assumed the interfacial velocity on drop surfaces (in an appropriate reference frame) and surfactant distribution to be axisymmetric in the gap region, both varying on the usual lubrication scale $a_i\delta^{1/2}$ along the gap. Two modes of mutual approach were predicted and quantified, 'rapid coalescence' (for a sufficiently strong driving force) on a time scale commensurate with

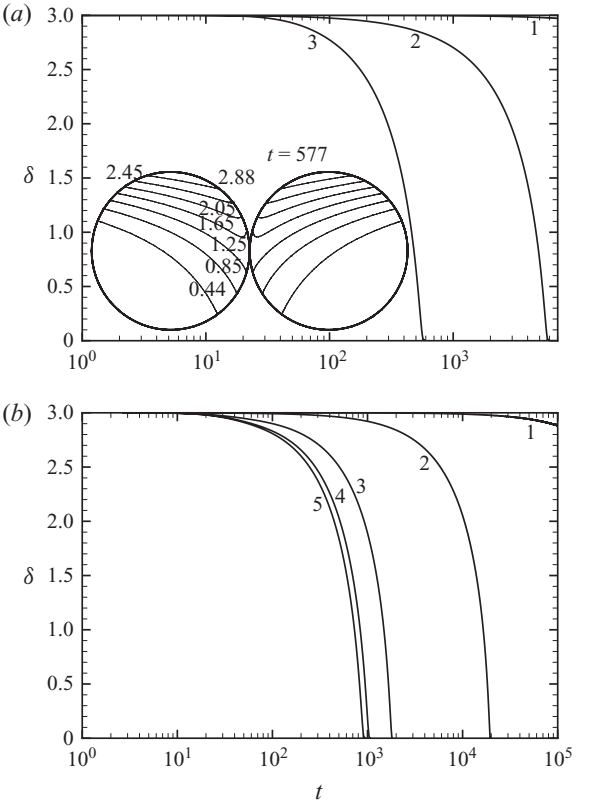

FIGURE 11. Evolution of the gap Δ between two equal-sized surfactant-covered spherical drops with $\widehat{\mu}=1$ and $Ma=0.1$ for sedimentation (a) normal to and (b) along the line of centres at different surface Péclet numbers: 1, $Pe_s=1$; 2, $Pe_s=10$; 3, $Pe_s=100$; 4, $Pe_s=500$; 5, $Pe_s=5000$. Initial gap is three drop radii. The inset in (a) is the drops' image for $Pe_s=100$ at the gap of 0.0001, which occurs at $t=577$. The contours indicate iso-concentration lines.

that for clean drops, and long-time approach (for a subcritical driving force) when the film drainage may be even slower than for rigid spheres. Since $|\boldsymbol{V}_2-\boldsymbol{V}_1|\sim\delta^{1/2}$ in our simulations for figure 12, this case appears to be characteristic of 'rapid coalescence'. Besides small, but finite diffusion, though, the present asymmetric case has additional complications. Figure 13 (solid lines) presents the distribution of surfactant along the gap for drop 1 in the plane $y_1=y_2=0$, as a function of a stretched variable $x_1\delta^{-1/2}$ for the near-contact stage of simulation in figures 11(a) and 12 at $Pe_s=100$; the axis x_1 is defined in figure 1 and is (for the given case) antiparallel to the direction of the doublet motion. For comparison, dashed lines show an analogous simulation with less diffusion ($Pe_s=500$). All curves were calculated for azimuthal truncation $M=8$ (§3.3) and found to be graphically indistinguishable from those for $M=4$; variation of ε-parameter (controlling the order of harmonics retained, §3.3) confirms excellent numerical convergence of the results in figure 13. The range $|x_1\delta^{-1/2}|\leqslant 8$ essentially limits the data to near-contact region, both for $\delta=0.001$ and 3×10^{-5}. Axial symmetry of surfactant distribution in the gap would imply the symmetry of the curves in figure 13 about $x_1\delta^{-1/2}=0$, which is not observed, even approximately. Despite this unexpected conclusion, indicating substantial difficulty of asymptotic analysis for the present case, the results in figure 13 help to explain the behaviour of

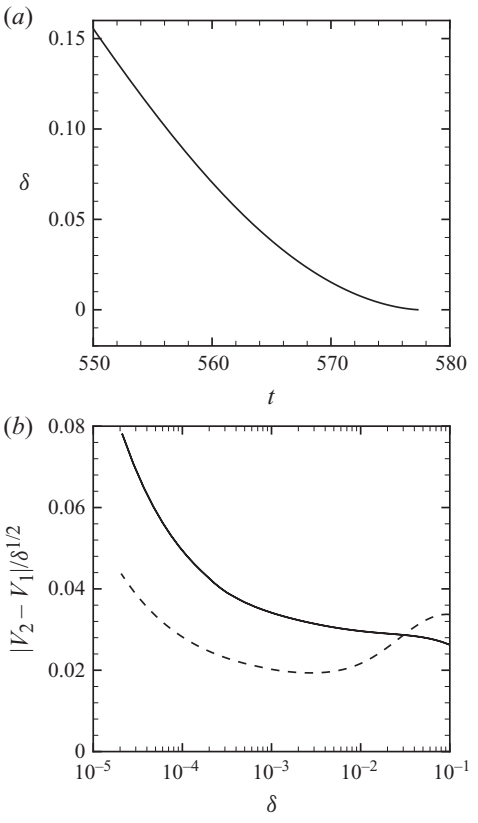

FIGURE 12. Near-contact behaviour for the two-drop sedimentation normal to the line of centres from figure 11(*a*) at $Pe_s = 100$ (solid lines). In (*b*), the relative velocity $|\boldsymbol{V}_2 - \boldsymbol{V}_1|$ along the line of centres is scaled with the square root of the gap; the dashed line is for an analogous simulation at a different Péclet number, $Pe_s = 500$.

the relative velocity in figure 12(*b*). Namely, as collision is approached, Γ becomes an increasingly smooth function of $x_1\delta^{-1/2}$ (and $y_1\delta^{-1/2}$), the role of Marangoni stresses in the gap hampering mutual approach is reduced, and $|\boldsymbol{V}_2 - \boldsymbol{V}_1|\delta^{-1/2}$ increases sharply. For $Pe_s = 500$, due to larger Marangoni stresses in the gap, the near-contact approach velocity $|\boldsymbol{V}_2 - \boldsymbol{V}_1|$ is roughly half of that for $Pe_s = 100$ (figure 12*b*). On the contrary, at the initial stage $\delta \geqslant 0.03$, larger Marangoni stresses on the entire drop surfaces for $Pe = 500$ produce a larger driving force and faster mutual approach, compared to the case $Pe_s = 100$. The overall collision time $t = 478$ for $Pe_s = 500$ is only slightly shorter than $t = 577$ for $Pe_s = 100$. Although an analytical theory of surfactant-enhanced coalescence is still lacking, we have been able to verify the direction of relative motion for the simulation in figure 12(*a*) using the boundary-integral algorithm of Rother *et al.* (2006) at $\widehat{\mu} = 1$, $Pe_s = 100$ and finite, but small deformation.

Enhanced coalescence phenomenon for two equal drops sedimenting along the line of centres (figure 11*b*) at high Péclet numbers presents an interesting case, where a nearly stagnant cap of surfactant and a clean spot include the lubrication area. Referring to figure 1, where drop 1 is assumed to be strictly below drop 2 (and both sediment downwards), figure 14 presents the axisymmetrical distribution of surfactant versus θ_1 (or θ_2) angle on both surfaces at $\delta = 3 \times 10^{-5}$ and $Pe_s = 100$, 500 and 20 000. The $Pe_s = 5000$ result is almost indistinguishable from that for $Pe_s = 20\,000$ and is

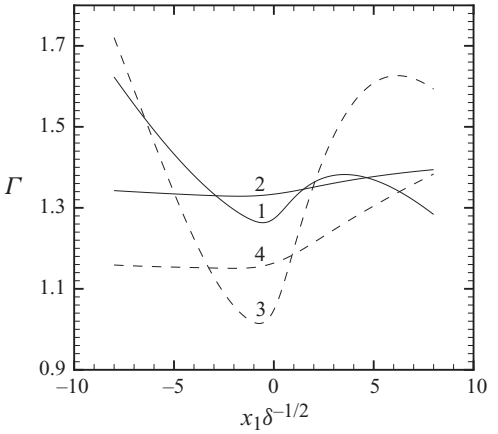

FIGURE 13. Distribution of surfactant along the gap for the sedimentation of two equal drops normal to the line of centres from figures 11(*a*) and 12. Solid lines, $Pe_s = 100$; dashed lines, $Pe_s = 500$. Curves 1 and 3 are for surface separation $\delta = 0.001$; curves 2 and 4 are for $\delta = 3 \times 10^{-5}$.

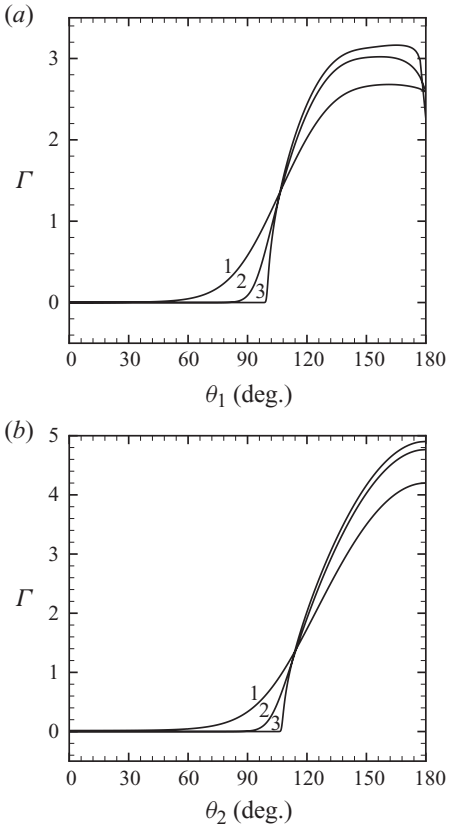

FIGURE 14. Distribution of surfactant on the surfaces of (*a*) the leading and (*b*) the trailing drop of equal radii in their sedimentation along the line of centres in near contact ($\delta = 3 \times 10^{-5}$). Curves: 1, $Pe_s = 100$; 2, $Pe_s = 500$; 3, $Pe_s = 20\,000$; other parameters and initial conditions are the same as in figure 11(*b*).

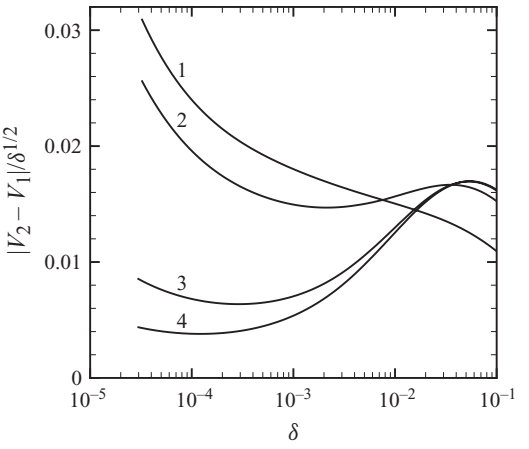

FIGURE 15. Relative velocity, scaled with $\delta^{1/2}$, for two equal drops sedimenting along the line of centres at $\hat{\mu} = 1$, $Ma = 0.1$ and different Péclet numbers: 1, $Pe_s = 100$; 2, $Pe_s = 500$; 3, $Pe_s = 5000$; 4, $Pe_s = 20\,000$.

not shown. Although the process is not quite steady state, nearly stagnant caps of surfactant are formed as $Pe_s \to \infty$, on the leading and trailing drops, with cap angles $\theta_1^c \approx 98^\circ$ and $\theta_2^c \approx 106^\circ$, respectively; the rest of each drop is free from surfactant. In this limit, the surfactant distributions are still continuous, with infinite derivatives $\mathrm{d}\Gamma/\mathrm{d}\theta_i$ at the transition points to clean spots. Due to interaction, surfactant distributions are quite different for the leading and trailing drops; squeezing flow results in sharp variation and non-monotonic behaviour of Γ on drop 1 in the near-contact area (figure 14). The calculations proceed much faster than for a general three-dimensional case, since the azimuthal truncation $M = 0$ suffices due to axial symmetry. For the purposes of high accuracy, the order n of harmonics was limited from below by 20, 40, 100 and 300 for $Pe_s = 100$, 500, 5000 and 20 000, respectively. This is essential at the initial stage of simulation, until the interaction-based truncation scheme of § 3.3 with $\varepsilon = 0.001$ comes into play, eventually making n reach several hundred. Halving these bounds and coarsening ε to 0.002 produced the results graphically indistinguishable from those in figure 14. High order of harmonics is essential at $Pe_s \gg 1$ to avoid grossly negative Γ in the 'clean-spot' area, but reasonably small negative Γ have no appreciable effect on global drop dynamics (and surfactant distribution in the caps) and can be tolerated; generally, it makes no sense to resolve extremely small concentrations in the clean-spot area. High-accuracy calculations in figure 14, though, have avoided negative Γ altogether (with $\Gamma \sim 10^{-6}$–10^{-7} in the clean spots at $Pe_s = 20\,000$).

For these simulations at the near-collision stage, the relative drop velocity scaled with $\delta^{1/2}$ is shown in figure 15. At $Pe_s = \infty$, the near-contact interaction would resemble that between a perfectly rigid sphere and a clean drop, with a $|\boldsymbol{V}_2 - \boldsymbol{V}_1| \sim \delta$ behaviour. It follows from figure 15, however, that this limit can be achieved only at extremely large Péclet numbers. For $Pe_s \leqslant 5000$, with small but appreciable tangential velocity on the capped portion of the leading drop, the behaviour of the relative velocity is still closer to that for two clean drops ($|\boldsymbol{V}_1 - \boldsymbol{V}_2| \sim \delta^{1/2}$); for $Pe_s = 20\,000$, the $|\boldsymbol{V}_2 - \boldsymbol{V}_1| \sim \delta$ behaviour is roughly observed for $\delta \geqslant 10^{-3}$ only. It may be possible to apply the local lubrication analysis of Cristini *et al.* (1998) and Bławzdziewicz *et al.* (1999*a*) to this axisymmetric case for a semi-analytical description, but an

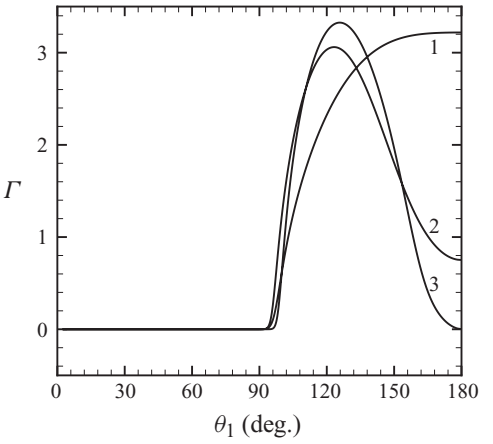

FIGURE 16. Evolution of surfactant concentration in the cap on the smaller (leading) drop, as collision is approached between two unequal drops sedimenting along the line of centres at $k = 0.5$, $\hat{\mu} = 1$, $Ma = 0.025$ and $Pe_s = 20\,000$. Curves: 1, $\delta = 2$; 2, $\delta = 0.1$; 3, $\delta = 3 \times 10^{-5}$.

extension must be made for a diffusive surfactant; it follows from figure 15 that the role of surface diffusion increases as collision is approached. Using their method would require a numerical solution of a stiff nonlinear partial differential equation for surfactant concentration in the lubrication area, with initial conditions provided by the present global solution at some small clearance δ, which is not a straightforward task. The necessary 'outer solution' would also require a modification of the present method, with a different iterative scheme, to allow the drop motion in near-contact with the same velocities $\boldsymbol{V}_1 = \boldsymbol{V}_2$, until a steady state is reached. Due to these complications, a near-contact asymptotic analysis goes beyond the scope of the present paper, but may be a subject of future research.

The following example demonstrates a typical scenario for two unequal drops settling along the line of centres and covered with a low-diffusing surfactant at a small Marangoni number ($k = 0.5$, $\hat{\mu} = 1$, $Ma = 0.025$, $Pe_s = 20\,000$). As the drops approach contact from large distances ($\delta = 50$ initially), the surfactant distribution on the larger, trailing drop with a nearly-stagnant cap ($\theta_2^c \approx 134^\circ$) does not show any noticeable changes. The cap angle $\theta_1^c = 92^\circ$–96° on the smaller, leading drop varies only slightly, but the surfactant distribution in the cap is significantly altered by the squeezing flow (much stronger than for two equal drops under similar conditions) and, at collision, the lubrication area becomes entirely devoid of surfactant (figure 16). Due to clean spots on both sides of the gap, the approach velocity roughly follows the scaling $|\boldsymbol{V}_2 - \boldsymbol{V}_1| \sim \delta^{1/2}$ for all small separations.

Returning to general three-dimensional motion of unequal drops, a physical example of contaminated air bubbles rising through water is studied in figure 17. Physical properties for this system are $\rho_e = 1000\,\mathrm{kg\,m^{-3}}$, $\rho_d = 1204\,\mathrm{kg\,m^{-3}}$, $\mu_e = 0.001\,\mathrm{kg\,(m\,s)^{-1}}$, $\sigma_0 = 0.0728\,\mathrm{N\,m^{-1}}$, ideal gas constant $R = 8.3145\,\mathrm{J\,(mol\,K)^{-1}}$, gravitational acceleration $g = 9.8\,\mathrm{m\,s^{-2}}$ and absolute temperature $T = 293\,\mathrm{K}$. The surface diffusivity was taken equal to the bulk diffusivity and given a value of $D_s = 1 \times 10^{-9}\,\mathrm{m^2\,s^{-1}}$ (Shen *et al.* 2002; Hudson *et al.* 2003), where the bulk surfactant diffusivity is $O(10^{-10})$ to $O(10^{-9})\,\mathrm{m^2\,s^{-1}}$ (Shen *et al.* 2002). Because maximum deviation from the incompressible limit is expected at low surface concentrations, we choose $\Gamma_{eq} = 1 \times 10^{-9}\,\mathrm{mol\,m^{-2}}$ (Subramanian & Balasubramaniam 2001); this value is

a_2 (μm)	Re	Ca	Pe_s	Ma	A
5	0.0012	3.4×10^{-6}	1.2	10	12
10	0.0098	1.3×10^{-5}	9.8	2.5	24
20	0.078	5.4×10^{-5}	78	0.62	49
30	0.26	1.2×10^{-4}	260	0.28	73
40	0.63	2.2×10^{-4}	630	0.16	97
50	1.2	3.4×10^{-4}	1200	0.10	120

TABLE 1. Dimensionless groups for air bubbles in water.

much smaller than a typical maximum-packing concentration of 10^{-5}–10^{-6} mol m^{-2} (Shen *et al.* 2002), so an 'ideal-gas' model for surfactant is valid. The velocity for scaling U and definitions for the Reynolds number, Re, and capillary number, Ca, in terms of dimensional variables are

$$U = \frac{\Delta\rho g a_2^2}{\mu_e}, \quad Re = \frac{\rho_e U a_2}{\mu_e}, \quad Ca = \frac{\mu_e U}{\sigma^*}, \tag{4.4}$$

where $\sigma^* = \sigma_0 - RT\Gamma_{eq}$ is the interfacial tension reduced by the initially uniform surfactant surface concentration.

Table 1 provides information on the range of several dimensionless parameters for larger bubble radii a_2 between 5 and 50 μm. Restrictions on the current model include negligible inertia and deformation, i.e. small Re and Ca. The isolated sedimentation velocity of the larger drop velocity is less than U by a factor of 2/9 to 1/3, so that more appropriate Re and Ca would be smaller than the values in table 1. An additional limitation is that Brownian motion be negligible, which is met by bubbles greater than a few micrometres in diameter (Zhang & Davis 1991).

In figure 17, at smaller bubble radii, where the surface Péclet number is small, and the Marangoni number is large, the critical non-dimensional horizontal offset d_∞^* is close to the value determined for the incompressible surfactant limit. At larger a_2, Pe_s increases and Ma decreases (see table 1), so that d_∞^* is closer to the results for clean bubbles. At large enough bubble sizes, critical offsets from the current model nearly coincide with those for uncontaminated interfaces (beyond the results shown). In the intermediate bubble sizes, the most interesting behaviour is observed. In particular, for $k = 0.9$ in figure 17(*b*), d_∞^* is greater than the Smoluchowski value of 1.9 for a_2 greater than 25 μm, and the system exhibits the same surfactant-enhanced coalescence seen in the dimensionless parameter space. Calculations performed at a higher initial surfactant surface concentration of $\Gamma_{eq} = 1 \times 10^{-7}$ mol m^{-2} for $k = 0.5$ show that d_∞^* closely follows the incompressible surfactant limit (results not shown).

The neglect of drop deformation in the present calculations merits additional discussion. Although spherical drops with mobile surfaces collide under the action of finite forces (such as gravity), even a small amount of deformation would prohibit physical contact in a finite time, due to slow drainage of the film between the surfaces (Yiantsios & Davis 1990, 1991). Singular van der Waals attraction, however, makes collisions possible even with deformation, so coalescence of two slightly deformable drops is a subtle interplay between the two, small-scale factors acting in opposite directions. For glancing collisions of clean drops at $0 < Ca \ll 1$, Rother, Zinchenko & Davis (1997) developed an asymptotic approach by matching the axisymmetrical local thin-film solution in the gap with the outer solution for two spherical drops in a three-dimensional motion; this approach, although sometimes questioned in

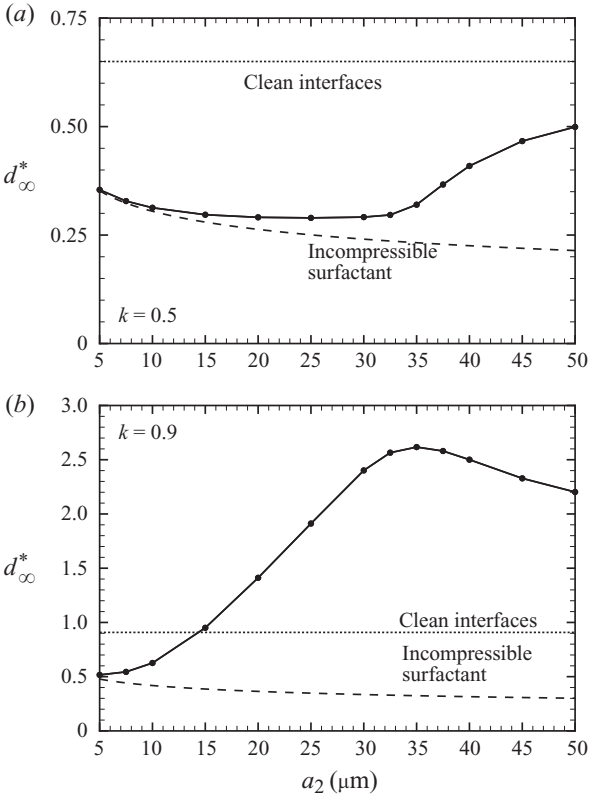

FIGURE 17. The dimensionless critical horizontal offset versus the larger drop radius a_2 in microns for a physical system of air bubbles in water ($\widehat{\mu} = 0$) for (*a*) $k = 0.5$ and (*b*) $k = 0.9$. In both (*a*) and (*b*), the upper, short-dashed horizontal line is for clean drops ($A = 0$), while the lower, long-dashed curve marks results for incompressible surfactant. The solid lines are from the present, more general solution for compressible surfactant. The calculations for contaminated drops assume an equilibrium surfactant concentration of $\Gamma_{eq} = 1 \times 10^{-9}$ mol m^{-2}.

the literature, was completely justified by accurate full three-dimensional boundary-integral calculations at small *Ca* (Zinchenko & Davis 2005). Calculations of Rother *et al.* (1997, figure 16 therein) for typical Hamaker constant and surface tension show a negligible effect of deformation on collision efficiency for drops less than a few hundred micron. Even with surfactant, it is safe to neglect deformation for much smaller drops, as in our figure 17.

5. Concluding remarks

An algorithm has been developed to treat the gravity-induced three-dimensional collisions of two spherical drops covered with insoluble surfactant at low Reynolds numbers. Unlike in previous collision studies, our solution accounts for nonlinear coupling between the surfactant transport and drop hydrodynamics by solving the full convective–diffusion equation for the surfactant transport and is applicable at arbitrary Marangoni (*Ma*) and surface Péclet (Pe_s) numbers. The method includes twin multipole expansions with economical truncation for hydrodynamics and a Galerkin-type approach for surfactant transport. Our solution is capable of accurately calculating thousands of trajectories from large separation to very close contact

($\delta \sim 10^{-4}$) and is used to determine collision efficiencies by trial and error in a wide range of parameters, including the case of small, but finite, surface diffusion ($Pe_s \sim 10^3$–10^4). Selected examples show how stagnant-cap surfactant distributions, observed for $Ma \ll 1$ and $Pe_s \gg 1$, are affected by hydrodynamical interactions and the squeezing flow. For finite drop-to-medium viscosity ratios, as collision is approached, the relative velocity scaling is typically the same as for two clean drops, which enables contact in a finite time without van der Waals forces not included in the present analysis. For moderate size ratios, drop behaviour is generally bounded by that of clean drops and that of drops with nearly uniform surfactant coverage. At larger size ratios, nonlinear coupling between surfactant dynamics and flow leads to collision efficiencies that even exceed the geometrical Smoluchowski value. Related, this nonlinear coupling causes equal-sized drops to migrate towards each other and collide. These novel effects do not exist for clean spherical drops or in the incompressible surfactant approximation.

These results are surprising in that surfactants are often used to stabilize emulsions, while we observe that coalescence can also be enhanced by surfactants for drops with size ratio close to unity. Future studies must address the overall effect of this coalescence enhancement on the drop-size evolution through population-dynamics simulations. The surfactant-enhanced coalescence is observed only at low surface concentrations, as our calculations for a model system of contaminated air bubbles in water demonstrate. In addition, bulk solubility of the surfactant would likely lead to smaller gradients in the surfactant concentration (Pawar & Stebe 1996; Eggleton *et al.* 2001) and a weakening of the effect. That is, longer times might be required for coalescence to occur. The implications of these findings for flow-induced collisions are unclear at present. The external flow might mask the phenomenon, as in the case of deformation-enhanced coalescence of clean deformable drops (Manga & Stone 1993, 1995), which is observed in buoyancy flow but not shear. Further investigation into the interactions and collisions of two contaminated spherical drops in linear flows, such as shear, with compressible surfactant should be made. This computationally demanding problem may require an even more efficient algorithm, by combining the present techniques with high-order near-contact lubrication analysis.

The work of M.A.R. was supported by the Office of the Vice President for Research at the University of Minnesota. M.A.R. would like to thank the VDIL at UMD and the Minnesota Supercomputing Institute for use of computing resources.

Appendix. Rate of convergence of multipole expansions

To demonstrate the correctness of the progression exponents (3.27), consider the simplest classical problem, which can be solved both by twin spherical expansions and by the method of images, namely, steady heat transfer between two spheres S_1 and S_2 with prescribed temperatures T_1 and T_2. Using the latter, well-known method, two infinite systems $\mathscr{A}_1 = \{\boldsymbol{P}_1^1, \boldsymbol{P}_2^1, \ldots\}$ and $\mathscr{A}_2 = \{\boldsymbol{P}_1^2, \boldsymbol{P}_2^2, \ldots\}$ of image points inside S_1 and S_2, respectively, are constructed, so that $\boldsymbol{P}_1^\gamma = \boldsymbol{O}_\gamma$ and $\boldsymbol{P}_{k+1}^{\gamma+1}$ is the inversion of $\boldsymbol{P}_k^\gamma$ with respect to $S_{\gamma+1}$ (figure 18); indices γ and $\gamma+1$ are reduced by module 2.

By construction

$$\left|\boldsymbol{P}_{k+1}^{\gamma+1} - \boldsymbol{O}_{\gamma+1}\right| \cdot \left|\boldsymbol{P}_k^\gamma - \boldsymbol{O}_{\gamma+1}\right| = a_{\gamma+1}^2, \tag{A 1}$$

so

$$\left|\boldsymbol{x} - \boldsymbol{P}_{k+1}^{\gamma+1}\right| \cdot \left|\boldsymbol{O}_{\gamma+1} - \boldsymbol{P}_k^\gamma\right| = a_{\gamma+1}\left|\boldsymbol{x} - \boldsymbol{P}_k^\gamma\right|, \tag{A 2}$$

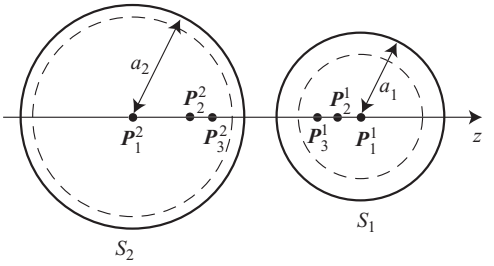

FIGURE 18. The image system for two interacting spheres. All the image points $\boldsymbol{P}_k^\gamma$ inside S_γ approach the limiting spheres $|\boldsymbol{P}-\boldsymbol{O}_\gamma|=a_\gamma q_\gamma$ (dashed lines), as $k\to\infty$.

for all $\boldsymbol{x}\epsilon S_{\gamma+1}$. The solution for the temperature outside the spheres is

$$T^e(\boldsymbol{x})=\sum_{\gamma=1}^{2}\sum_{k=1}^{\infty}\frac{Q_k^\gamma}{|\boldsymbol{x}-\boldsymbol{P}_k^\gamma|}, \tag{A 3}$$

with $Q_1^\gamma=a_\gamma T_\gamma$ and other coefficients found recurrently to satisfy the boundary conditions. Each term in (A 3) can be re-expanded in the standard way into multipoles centred at $\boldsymbol{O}_\gamma$. Then comparing the result with a twin spherical expansion (cf. (3.2)–(3.4)),

$$T^e(\boldsymbol{x})=T_-^1+T_-^2=\sum_{\gamma=1}^{2}\sum_{n=0}^{\infty}A_{-(n+1),0}^{\gamma}\left(\frac{a_\gamma}{r_\gamma}\right)^{n+1}Y_{n,0}(\boldsymbol{r}_\gamma), \tag{A 4}$$

gives the coefficients

$$A_{-(n+1),0}^{\gamma}=\frac{(-1)^{n\gamma}}{a_\gamma}\left(\frac{4\pi}{2n+1}\right)^{1/2}\sum_{k=1}^{\infty}Q_k^\gamma\left(\frac{|\boldsymbol{P}_k^\gamma-\boldsymbol{O}_\gamma|}{a_\gamma}\right)^n. \tag{A 5}$$

As $k\to\infty$, the image points $\boldsymbol{P}_k^\gamma$ approach limiting positions $\boldsymbol{P}_\infty^1$ and $\boldsymbol{P}_\infty^2$ for $\gamma=1$ and 2, respectively (which are nothing but the poles of the bispherical coordinate system for S_1 and S_2), and the progression exponent q_γ for the decay of $A_{-(n+1),0}^{\gamma}$, as $n\to\infty$, is obviously $|\boldsymbol{P}_\infty^\gamma-\boldsymbol{O}_\gamma|/a_\gamma$. Simple algebra yields the explicit expressions (3.27) for q_1 and q_2.

Using the more complex asymptotic technique (Zinchenko 1994, Appendix B), it can be shown that the progression exponents (3.27) are quite universal. They describe the decay of multipole coefficients (to within an algebraic factor n^α) in non-axisymmetrical problems as well, for Laplace and Stokes equations in a two-sphere geometry.

REFERENCES

AGRAWAL, S. & WASAN, D. 1979 The effect of interfacial viscosities on the motion of drops and bubbles. *Chem. Engng J.* **18**, 215–223.

ALVES, S. S., ORVALHO, S. P. & VASCONCELOS, J. M. T. 2005 Effect of bubble contamination on rise velocity and mass transfer *Chem. Engng Sci.* **60**, 1–9.

BEITEL, A. & HEIDEGGER, W. J. 1971 Surfactant effects on mass transfer from drops subject to interfacial instability. *Chem. Engng Sci.* **26**, 711–717.

BŁAWZDZIEWICZ, J., CRISTINI, V. & LOEWENBERG, M. 1999*a* Near-contact motion of surfactant-covered spherical drops: ionic surfactant. *J. Colloid Interface Sci.* **211**, 355–366.

BŁAWZDZIEWICZ, J., WAJNRYB, E. & LOEWENBERG, M. 1999*b* Hydrodynamic interactions and collision efficiencies of spherical drops covered with an incompressible surfactant film. *J. Fluid Mech.* **395**, 29–59.

Bławzdziewicz, J., Vlahovska, P. & Loewenberg, M. 2000 Rheology of a dilute emulsion of surfactant-covered spherical drops. *Physica* A **276**, 50–85.

Chen, J. & Stebe, K. J. 1996 Marangoni retardation of the terminal velocity of a settling droplet: the role of surfactant physico-chemistry. *J. Colloid Interface Sci.* **178**, 144–155.

Chesters, A. K. & Bazhlekov, I. B. 2000 Effect of insoluble surfactants on drainage and rupture of a film between drops interacting under a constant force. *J. Colloid Interface Sci.* **230**, 229–243.

Cichocki, B., Felderhof, B. U. & Schmitz, R. 1988 Hydrodynamic interactions between two spherical particles. *Physico-Chem. Hydrodyn.* **10**, 383–403.

Cristini, V., Bławzdziewicz, J. & Loewenberg, M. 1998 Near-contact motion of surfactant-covered spherical drops. *J. Fluid Mech.* **366**, 259–287.

Cristini, V. & Tan, Y. 2004 Theory and numerical simulation of droplet dynamics in complex flows – a review. *Lab on a Chip* **4**, 257–264.

Cuenot, B., Magnaudet, J. & Spennato, B. 1997 The effects of slightly soluble surfactants on the flow around a spherical bubble. *J. Fluid Mech.* **339**, 25–53.

Danov, K. D., Valkovska, D. S. & Ivanov, I. B. 1999 Effect of surfactants on the film drainage. *J. Colloid Interface Sci.* **211**, 291–303.

Davis, R. H., Schonberg, J. A. & Rallison, J. M. 1989 The lubrication force between two viscous drops. *Phys. Fluids* **1**, 77–81.

Edge, R. M. & Grant, C. D. 1972 The motion of drops in water contaminated with a surface active agent. *Chem. Engng Sci.* **27**, 1709–1721.

Eggleton, C. D., Pawar, Y. & Stebe, K. J. 1999 Insoluble surfactants on a drop in an extensional flow: a generalization of the stagnated surface limit to deforming interfaces. *J. Fluid Mech.* **385**, 79–99.

Eggleton, C. D., Tsai, T. M. & Stebe, K. J. 2001 Tip streaming from a drop in the presence of surfactants. *Phys. Rev. Lett.* **87**, 048302.

Elzinga, E. R. & Banchero, J. T. 1961 Some observations on the mechanics of drops in liquid–liquid systems. *AIChE J.* **7**, 394–399.

Fdhila, R. & Duineveld, P. C. 1996 The effect of surfactants on the rise of a spherical bubble at high Reynolds and Peclet numbers. *Phys. Fluids* **8**, 310–321.

Frumkin, A. & Levich, V. 1947 O vliyanii poverkhnosto-aktivnikh veshestv na dvizhenie na granitse zhidkikh sred. *Zhur. Fizic. Khimii* **21**, 1183–1204.

Garner, F. H. & Skelland, H. P. 1955 Some factors affecting droplet behavior in liquid–liquid systems. *Chem. Engng Sci.* **4**, 149–158.

Griffith, R. 1962 The effect of surfactants on the terminal velocity of drops and bubbles. *Chem. Engng Sci.* **17**, 1057–1070.

Happel, J. & Brenner, H. 1973 *Low Reynolds Number Hydrodynamics*. Nijhoff.

Harper, J. F. 1988 The near stagnation region of a bubble rising steadily in a dilute surfactant solution. *Q. J. Mech. Appl. Math.* **41**, 204–213.

Harper, J. F. 2007 Bubble rise in a liquid with a surfactant gas in particular carbon dioxide *J. Fluid Mech.* **581**, 157–165.

He, Z., Maldarelli, C. & Dagan, Z. 1991 The size of stagnant caps of bulk soluble surfactant on the interfaces of translating liquid droplets. *J. Colloid Interface Sci.* **146**, 442–451.

Hetsroni, S. & Haber, S. 1978 Low Reynolds number motion of two drops submerged in an unbounded arbitrary velocity field. *Intl J. Multiphase Flow* **4**, 1–17.

Holbrook, J. A. & LeVan, M. D. 1983*a* Retardation of droplet motion by surfactant. Part 1. Theoretical development and asymptotic solutions. *Chem. Engng Commun.* **20**, 191–207.

Holbrook, J. A. & LeVan, M. D. 1983*b* Retardation of droplet motion by surfactant. Part 2. Numerical solutions for exterior diffusion, surface diffusion, and adsorption kinetics. *Chem. Engng Commun.* **20**, 273–290.

Horton, T. J., Fritsch, T. R. & Kintner, R. C. 1965 Experimental determination of circulation velocities inside drops. *Can. J. Chem. Engng* **43**, 143–146.

Hu, Y. T., Pine, D. J. & Leal, L. G. 2000 Drop deformation, breakup, and coalescence with compatibilizer. *Phys. Fluids A* **12**, 484–489.

Hudson, S. D., Jamieson, A. M. & Burkhart, B. E. 2003. The effect of surfactant on the efficiency of shear-induced drop coalescence, *J. Colloid Interface Sci.* **265** (2), 409–421.

Jones, R. B. & Schmitz, R. 1988 Mobility matrix for arbitrary spherical particles in solution. *Physica* A **149**, 373–394.

KARSA, D. R. (Ed.) 2000 *Surface Active Behaviour of Performance Surfactants*. Sheffield Academic Press.

KORN, G. A. & KORN, T. M. 1968 *Mathematical Handbook for Scientists and Engineers*. McGraw-Hill.

KUSHNER, J. IV, ROTHER, M. A. & DAVIS, R. H. 2001 Buoyancy-driven interactions of viscous drops with deforming interfaces. *J. Fluid Mech.* **446**, 253–269.

LEVICH, A. 1962 *Physiochemical Hydrodynamics*. Prentice Hall.

LI, D. 1996 Coalescence between small bubbles: effects of surface tension gradient and surface viscosities. *J. Colloid Interface Sci.* **181**, 34–44.

LI, X. & MAO, Z. 2001 The effect of surfactant on the motion of a buoyancy-driven drop at intermediate Reynolds numbers: a numerical approach. *J. Colloid Interface Sci.* **240**, 307–322.

LI, X. & POZRIKIDIS, C. 1997 The effect of surfactants on drop deformation and on the rheology of dilute emulsions in Stokes flow. *J. Fluid Mech.* **341**, 165–194.

MANGA, M. & STONE, H. A. 1993 Buoyancy-driven interactions between two deformable viscous drops. *J. Fluid Mech.* **256**, 647–683.

MANGA, M. & STONE, H. A. 1995 Collective hydrodynamics of deformable drops and bubbles in dilute low Reynolds number suspensions. *J. Fluid Mech.* **300**, 231–263.

MO, G. & SANGANI, A. S. 1994 A method for computing Stokes flow interactions among spherical objects. *Phys. Fluids* **6**, 1637.

MOUSA, H. & VAN DE VEN, T. G. M. 1991 Stability of water-in-oil emulsions in simple shear flow. Part 2. The effects of additives on the orthokinetic coalescence efficiency. *Colloids Surf.* A **60**, 39–51.

NANDI, A., MEHRA, A. & KHAKHAR, D. V. 1999 Suppression of coalescence in surfactant stabilized emulsions by shear flow. *Phys. Rev. Lett.* **83**, 2461–2464.

NGUYEN, N. & WERELY, S. T. 2002 *Fundamentals and Applications of Microfluidics*. Artech House.

PARK, C. C., BALDESSARI, F. & LEAL, L. G. 2003 Study of molecular weight effects on coalescence: interface slip layer. *J. Rheol.* **47**, 911–942.

PAWAR, Y. & STEBE, K. J. 1996 Marangoni effects on drop deformation in an extensional flow: the role of surfactant physical chemistry. Part I. Insoluble surfactants. *Phys. Fluids* **8**, 1738.

PORTER, M. R. (Ed.) 1990 *Recent Developments in the Technology of Surfactants*. Elsevier Applied Science.

POZRIKIDIS, C. 1994 Effects of surface viscosity on the finite deformation of a liquid drop and the rheology of dilute emulsions in simple shearing flow. *J. Non-Newtonian. Fluid Mech.* **51**, 161–178.

ROTHER, M. A. 2009 Effects of incompressible surfactant on thermocapillary interactions of spherical drops. *Intl J. Multiphase Flow* **35**, 417–426.

ROTHER, M. A. & DAVIS, R. H. 1999 The effects of slight deformation on thermocapillary-driven droplet coalescence and growth. *J. Colloid Interface Sci.* **214**, 297–318.

ROTHER, M. A. & DAVIS, R. H. 2004 Buoyancy-driven coalescence of spherical drops covered with incompressible surfactant at arbitrary Péclet number *J. Colloid Interface Sci.* **270**, 205–220.

ROTHER, M. A., ZINCHENKO, A. Z. & DAVIS, R. H. 1997 Buoyancy-driven coalescence of slightly deformable drops. *J. Fluid Mech.* **346**, 117–148.

ROTHER, M. A., ZINCHENKO, A. Z. & DAVIS, R. H. 2006 Surfactant effects on buoyancy-driven viscous interactions of deformable drops. *Colloids Surf.* A **282–283**, 50–60.

SADHAL, S. S. & JOHNSON, R. E. 1983 Stokes flow past bubbles and drops partially coated with thin films. Part 1. Stagnant cap of surfactant film - exact solution. *J. Fluid Mech.* **126**, 237–250.

SAVILLE, D. 1973 The effect of interfacial tension gradients on droplet behaviour. *Chem. Engng J.* **5**, 251–259.

SHEN, A. Q., GLEASON, B., MCKINLEY, G. H. & STONE, H. A. 2002 Fiber coating with surfactant solutions. *Phys. Fluids* **14**, 4055–4068.

STONE, H. A. & LEAL, L. G. 1990 The effects of surfactants on drop deformation and breakup. *J. Fluid Mech.* **220**, 161–186.

STONE, H. A., STROOCK, A. D. & AJDARI, A. 2004 Engineering flows in small devices: microfluidics towards a lab-on-a-chip. *Annu. Rev. Fluid Mech.* **36**, 381–411.

SUBRAMANIAN, R. S. & BALASUBRAMANIAM, R. 2001. *The Motion of Bubbles and Drops in Reduced Gravity*. Cambridge University Press.

Takemura, F. 2005 Adsorption of surfactants onto the surface of a spherical rising bubble and its effect on the terminal velocity of the bubble. *Phys. Fluids* **17**, 048104.

Valkovska, D. S., Danov, K. D. & Ivanov, I. B. 1999 Surfactants role on the deformation of colliding small bubbles. *Colloids Surf.* A **156**, 547–566.

Valkovska, D. S., Danov, K. D. & Ivanov, I. B. 2000 Effect of surfactants on the stability of films between two colliding small bubbles. *Colloids Surf.* A **175**, 179–192.

Vlahovska, P., Bławzdziewicz, J. & Loewenberg, M. 2002 Nonlinear rheology of a dilute emulsion of surfactant-covered spherical drops in time-dependent flows. *J. Fluid Mech.* **463**, 1–24.

Wasserman, M. & Slattery, J. 1969 Creeping flow past a fluid globule when a trace of surfactant is present. *AIChE J.* **15**, 533–541.

Yamamoto, T. & Ishii, T. 1987 Effect of surface active materials on the drag coefficients and shapes of single large gas bubbles. *Chem. Engng Sci.* **42**, 1297–1303.

Yiantsios, S. G. & Davis, R. H. 1990 On the buoyancy-driven motion of a drop towards a rigid surface or a deformable interface. *J. Fluid Mech.* **217**, 547–573.

Yiantsios, S. G. & Davis, R. H. 1991 Close approach and deformation of two viscous drops due to gravity and van der Waals forces. *J. Colloid Interface Sci.* **144**, 412–433.

Yeo, L. Y., Matar, O. K., Perez de Ortiz, E. S. & Hewitt, G. F. 2001 The dynamics of Marangoni-driven local film drainage between two drops. *J. Colloid Interface Sci.* **241**, 233–247.

Zhang, X. & Davis, R. H. 1991 The rate of collisions of small drops due to Brownian or gravitational motion. *J. Fluid Mech.* **230**, 479–504.

Zhang, Y. & Finch, J. A. 2001 A note on single bubble motion in surfactant solutions. *J. Fluid Mech.* **429**, 63–66.

Zinchenko, A. Z. 1978 Calculation of hydrodynamic interaction between drops at low Reynolds numbers. *J. Appl. Math. Mech.* **42**, 1046–1051.

Zinchenko, A. Z. 1982 Calculations of the effectiveness of gravitational coagulation of drops with allowance for internal circulation. *J. Appl. Math. Mech.* **46**, 58–65.

Zinchenko, A. Z. 1994 An efficient algorithm for calculating multiparticle thermal interaction in a concentrated dispersion of spheres. *J. Comput. Phys.* **111**, 120–135.

Zinchenko, A. Z. & Davis, R. H. 2000 An efficient algorithm for hydrodynamical interaction of many deformable drops. *J. Comput. Phys.* **157**, 539–587.

Zinchenko, A. Z. & Davis, R. H. 2005 A multipole-accelerated algorithm for close interaction of slightly deformable drops. *J. Comput. Phys.* **207**, 695–735.

Zinchenko, A. Z. & Davis, R. H. 2008 Algorithm for direct numerical simulation of emulsion flow through a granular material. *J. Comput. Phys.* **227**, 7841–7888.

Zinchenko, A. Z., Rother, M. A. & Davis, R. H. 1999 Cusping, capture, and breakup of interacting drops by a curvatureless boundary-integral algorithm. *J. Fluid Mech.* **391**, 249–292.